M.Sc. Thesis

Aerosol Physics

Carbon dioxide emissions in past and future region of Jätkäsaari in Helsinki

Xiaoyu Li

22. 05. 2020

Supervisor: Leena Järvi

Reviewers: Leena Järvi and Timo Vesala

UNIVERSITY OF HELSINKI

MASTER'S PROGRAMME IN ATMOSPHERIC SCIENCES

P.O. BOX 64 (Gustaf Hällströmin katu 2)

FIN-00014 Helsingin yliopisto

HELSINGIN YLIOPISTO
HELSINGFORS UNIVERSITET
UNIVERSITY OF HELSINKI
MATEMAATTIS-LUONNONTIETEELLINEN TIEDEKUNTA
MATEMATISK-NATURVETENSKAPLIGA FAKULTETEN
FACULTY OF SCIENCE

Tiedekunta – Fakultet – Faculty	Koulutusohjelma – Utbildningsprogram – Degree programme
Faculty of Sciences	Master's Programme in Atmospheric Sciences

Opintosuunta – Studieinrikting – Study track
Aerosol Physics

Tekijä – Författare – Author
Xiaoyu Li

Työn nimi – Arbetets titel – Title
Carbon dioxide emissions in past and future region of Jätkäsaari in Helsinki

Työn laji – Arbetets art – Level	Aika – Datum – Month and year	Sivumäärä – Sidoantal – Number of pages
Master's thesis	05/2020	42

Tiivistelmä – Referat – Abstract

Urban areas account for 70% of worldwide energy-related CO_2 emissions and play a significant role in the global carbon budget. With the enhanced consumption of fossil fuel and the dramatic change in land use related to urbanization, control and mitigation of CO_2 emissions in the urban area is becoming a major concern for urban dwellers and city managers. It is of great importance and demand to estimate the local CO_2 emissions in urban areas to assess the effectiveness of mitigation regulation.

Surface Urban Energy and Water Balance Scheme (SUEWS) incorporated with a CO_2 exchange module provides an advanced method to model total urban CO_2 flux and quantify the different local-scale emission sectors involving transportation, human metabolism, buildings and vegetation. Using appropriate input data such as detailed site information and meteorological condition, it can simulate the local or neighbourhood scale CO_2 emissions in a specific period, or even under a future scenario.

In this study, the SUEWS model is implemented in an urban region, Jätkäsaari, which is an extension of Helsinki city centre, to simulate anthropogenic and biogenic CO_2 emissions in the past and future. The construction of this district started in 2009 and was planned to be completed in 2030. Therefore, this region is a good case to investigate the impacts of urban planning on urban CO_2 emissions. Based on the urban surface information, meteorological data, and abundant emission parameters, a simulation in this 1650 × 1400 m area with the spatial resolution of 50 × 50 m and the time resolution of an hour was conducted with the aim to get information on the total annual CO_2 emissions, and the temporal and spatial variability of CO_2 fluxes from different sources and sink in 2008 and 2030. The positive CO_2 fluxes indicate the CO_2 sources, while the negative indicate the CO_2 sinks.

In both of the previous and future case, the spatial variation of net CO_2 fluxes in Jätkäsaari is dominated by the distribution of traffic and human activities. From April to September, the vegetation acts as the CO_2 sink with negative net ecosystem exchange. In 2008, the modelled cumulative CO_2 flux is 3.0 kt CO_2 $year^{-1}$, consisting of 1.9 kt CO_2 $year^{-1}$ from metabolism, 1.9 kt CO_2 $year^{-1}$ from traffic, 0.5 kt CO_2 $year^{-1}$ from soil and vegetation respiration, as well as -1.3 kt CO_2 $year^{-1}$ from photosynthesis. In 2030, the total annual CO_2 emissions increase to 11.1 kt CO_2 $year^{-1}$ because of the rising traffic volume and amount of inhabitants. Road traffic became the dominant CO_2 sources, accounting for 53% of the total emissions. For the diurnal variation, in 2008, the study area remains the CO_2 sources with the exception of summertime morning when the net CO_2 flux is negative, while in 2030, the net CO_2 flux is positive in the whole day.

Avainsanat – Nyckelord – Keywords
Urban areas, Carbon dioxide flux, Urban planning, SUEWS

Säilytyspaikka – Förvaringställe – Where deposited
Kumpula Science Library

Muita tietoja – Övriga uppgifter – Additional information

Contents

1 Introduction

Carbon dioxide (CO_2) is the most important greenhouse gas released to the atmosphere by human activities and it is responsible for the ongoing global warming due to its abundant concentration and long lifetime (IPCC, 2014). It absorbs the outgoing long-wave radiation and re-emits part of the absorbed radiation back to the earth's surface. CO_2 is a natural part in the atmosphere as part of the earth's carbon cycle. Human activities affect the carbon cycle by injecting more CO_2 into the atmosphere and interfering the removal and storage ability of CO_2 sinks. As a result of industrialization and human activities, the global average CO_2 concentration in the atmosphere has increased from 280 ppm before industrial revolution to 407 ppm in 2018 (Blunden and Arndt, 2019).

Urban regions play a significant role in the global carbon budget. Despite urban areas only cover a small part of the earth's surface, more than 50% of people in the world live in cities (Kennedy at al. 2009). Urban regions are responsible for 75–80% of global greenhouse gas emissions (Satterthwaite, 2008), and account for around 70% of total energy-related CO_2 emissions worldwide (IEA, 2008). The CO_2 emissions can be divided into the anthropogenic and natural. Fossil fuel combustion and industrial processes are dominant anthropogenic CO_2 sources, which contributed to 78% of the global greenhouse gas emission increase (IPCC, 2014). At present, typical observed mixing ratio of CO_2 concentration in the urban boundary layer is around 400-450 ppm (Oke et al., 2017). Within cities, the major anthropogenic CO_2 sources are the human metabolism and combustion of fossil fuel related to traffic, industry, home heating or cooling, and building energy use. Green areas in cities act as CO_2 natural sources by respiration and sinks by vegetation photosynthesis (Christen et al., 2011). Green areas can be a robust predictor for net urban CO_2 fluxes. When the natural fraction reaches 80% in an urban area, the urban CO_2 emission can be neutralized by the vegetation sink (Nordbo et al., 2012).

Monitoring urban CO_2 emissions is an essential and urgent need for decision makers to verify whether implemented regulation or mitigation policies are effective. Eddy covariance (EC) technique is a common and direct approach to observe the CO_2 flux in urban region (Baldocchi et al., 2003). However, there are still some limitations. For example, EC technique measures the total CO_2 emissions rather than identifying specific sources and sinks, such as transportation and vegetation. In some urban regions with huge CO_2 emissions, the estimation of anthropogenic CO_2 fluxes is always based on the emission inventories (Brondfield et al.,

2012), which are the fundamental to evaluate trends of greenhouse gas emissions. Emission inventories contain high uncertainties both in the aggregated CO_2 emission estimation and in the temporospatial distribution of CO_2 emissions (Gately and Hutyra, 2017). The effectiveness of emission inventories depends on its accuracy associated with the spatial and temporal resolution, and informativeness (Velasco et al. 2014). Recently, considerable progresses have been made in simulating urban CO_2 emissions with model methods. Atmospheric inversion techniques, which combine the observed CO_2 flux and the mesoscale atmospheric transport model, have been developed to simulate urban CO_2 emissions and to validate the estimates of emission inventories (Feng et al., 2016; Lauvaux et al., 2016). Another potential method is to use a local or neighbourhood scale model to simulate the CO_2 fluxes from different sectors. For instance, the urban land surface model SUEWS (Surface Urban Energy and Water Balance Scheme, Järvi et al., 2011) incorporated with the CO_2 exchange module can be implemented to estimate both anthropogenic and biogenic CO_2 fluxes (Järvi et al., 2019). This kind of inventory-based modelling method is the only feasible means for urban planners to estimate CO_2 emissions from various sources and evaluate the impact of different planning scenarios on the emissions in future neighborhoods.

The goal of this study is to investigate the CO_2 emissions from different sources in previous and future Jätkäsaari, Helsinki, and further to examine the effects of urban planning on the CO_2 emissions. According to Helsinki City Planning Department, the construction of study area is planned to complete in 2030. In this study, the different CO_2 emission components are simulated using the neighbourhood-scale SUEWS model incorporated with CO_2 module. The simulation is conducted in a 1650 m × 1400 m domain in 2008 and 2030. Furthermore, this study focuses on the implement of the model in a real case, and the pre-processing of urban surface information into model input.

2 Theoretical background

2.1 Urban boundary layer

The planetary boundary layer (PBL) is a portion of the atmosphere which is directly affected by the presence of the earth's surface. The boundary layer always responds to the surface forcings, such as the frictional drag, evaporation and transpiration, thermal mixing, and pollutant emissions with a timescale of an hour or less (Stull, 1988; Holton and Hakim, 2012). Thus, the properties of the surface determine the behavior of PBL. The thickness of boundary layer has spatial and temporal variation, ranging from hundreds of meters to several kilometers. The flow field in PBL is strongly affected by the interactions with the earth's surface. Horizontal transport of quantities such as moisture, heat, momentum, and pollutants is typically dominated by the mean wind, and vertical transport is governed by turbulence. Turbulence is one of the most important transport processes in boundary layer and it is a representative of the boundary layer (Stull, 2013).

The urban boundary layer (UBL) generates its own structure due to the particular urban surface. The horizonal scales of UBL can be divided into street (10-100 m), neighbourhood (100-1000 m), and city (10-20 km) level (Barlow, 2014). In the vertical, the lowest 10% of the urban boundary layer is the surface layer, which consists of two parts: inertial sublayer and roughness sublayer (Figure 2.1). The urban roughness sublayer is defined as two to five times the mean height of urban buildings and trees, where the wind flow is dominated by the roughness of surface individual elements. The lowest part from the ground to rooftop level of urban roughness sublayer is urban canopy layer, where individual obstacle affects the generation of roughness and turbulence, and consequently, determines the complex flow (Arnfield, 2002; Oke et al., 2017). Above the roughness sublayer, there is the inertial sublayer. In this layer, the turbulence blends the effects of individual roughness elements, and the wind profile is logarithmic. Since in this layer the vertical variation of fluxes is small (typically <10%), it is also known as the constant flux layer (Wang et al., 2014). The mixed layer is above the surface layer, where the atmospheric properties including temperature, wind speed, and concentrations, are well-mixed due to the effects of strong fluxes. At nighttime, it corresponds to a nocturnal stable layer and a residual layer above. In the mixed layer, the thermal turbulence homogenizes the atmospheric properties, such as potential temperature, moisture, wind speed, uniformly in the vertical. It is capped by the inversion or the entrainment zone to block the influences of the surface to the free atmosphere. (Barlow, 2014; Oke et al., 2017).

The energy balance of urban boundary layer has its own characteristics, which are mostly defined by the impervious artificial materials of urban buildings and pavements, the low fraction of vegetation in land cover, and the anthropogenic heat (Ryu and Baik, 2011; Barlow, 2014). Compared to the non-urban areas, such as a rural or forest one, the sensible heat flux is higher, while the latent heat flux is lower in urban regions. The large thermal inertia of urban surfaces increases the storage heat flux. The short-wave radiation flux is affected by the reflection of construction surfaces and the outgoing infrared radiation is governed by the emissivity of materials. In addition, the contribution of rising anthropogenic heat released from vehicles and constructions to energy balance is noteworthy. Thus, the energy balance of urban boundary layer leads to the urban heat island, as well as the special evolution and structure of urban boundary layer (Barlow, 2014; Oke et al., 2017).

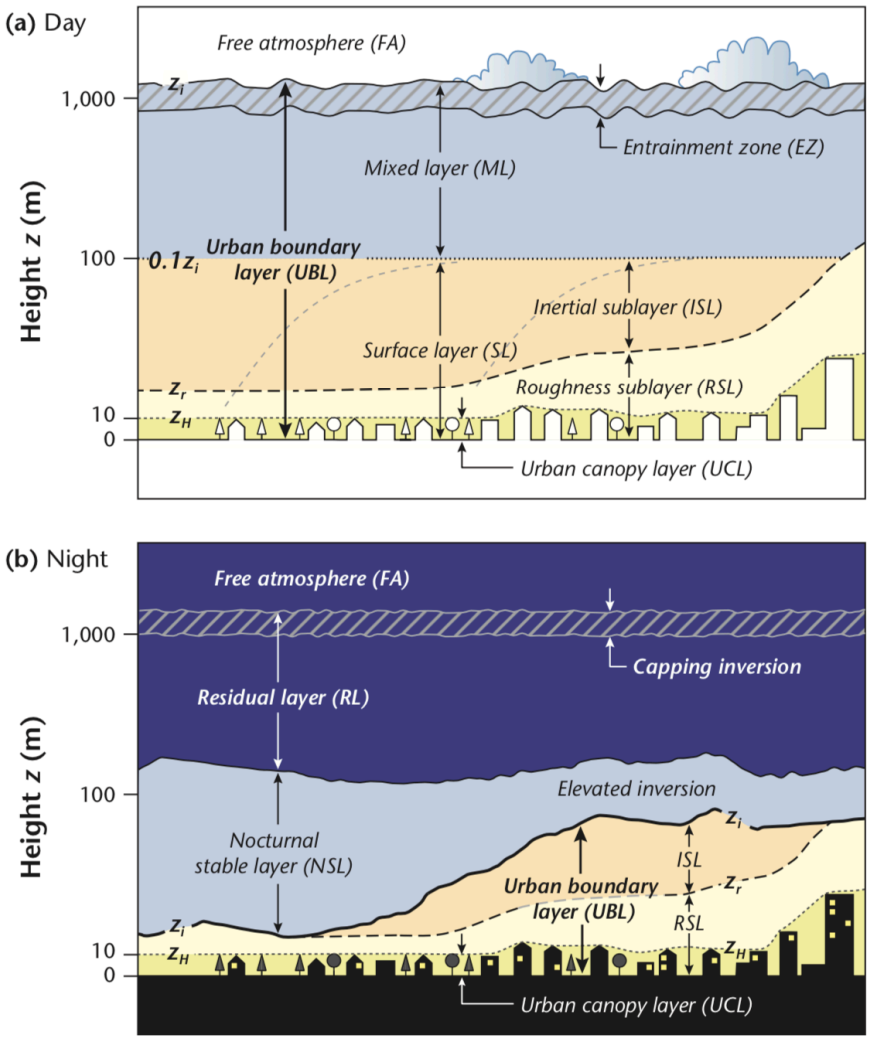

Figure 2.1 Schematic of typical layering of urban boundary layer at (a) daytime, and (b) nighttime. The height scale is logarithmic above 10 meters (Oke et al., 2017).

2.2 CO2 flux in urban areas

The exchange of CO_2 between urban surface and the atmosphere is driven by the vertical turbulent mixing in the UBL (Pino and Arellano, 2010), which can be measured using the eddy covariance (EC) technique or simulated by urban land surface models. The EC technique is widely used for the direct observation of turbulence fluxes of momentum, sensible heat, latent heat, and CO_2 (Nordbo et al., 2012). This micrometeorological method measures the covariance between vertical wind velocity fluctuations and CO_2 mixing ratio (Baldocchi et al., 2003). It should be implemented in the inertial sublayer to ascertain that the measurement represents a neighborhood level surface exchange and neglect the advection influences. EC measurements have been demonstrated to offer a relative accurate approach to evaluate the modelling results of CO_2 flux and to assess the CO_2 emissions inventories (Christen et al. 2011; Ward et al., 2015).

In urban areas, combustion of fossil fuels, such as coal, natural gas and petroleum contributes to most of CO_2 emissions. CO_2 is produced as a by-product through oxidation during the combustion processes including traffic, industry and home heating. The living organisms, such as humans and vegetation, oxidize organic material for energy and emit CO_2 to the atmosphere. Plants assimilate atmospheric carbon during the daytime through photosynthesis so that they act as CO_2 sinks in urban regions. (Lin et al. 2018).

Table 2.1 summarizes some urban CO_2 emission studies as obtained from observations in different cities since 2011. Besides EC, various methods, such as inverse model, inventory method, and inventory-based bottom-up model, have been exploited to estimate the urban CO_2 flux and all of the studies have reported that urban areas are source of CO_2. For example, in London, the estimation of the annual carbon flux utilizing EC measurements was 12.7 kg C m^{-2} $year^{-1}$ in a dense urban region in 2011, which seemed to be reasonable compared to the results of National Atmospheric Emissions Inventory (13.0 kg C m^{-2} $year^{-1}$) (Ward et al., 2015).

Studies on the relationship between urban planning and CO_2 emission mainly focus on the impacts of urban forms, building types and areas, transport means, vegetation areas, plant community types, and population density on CO_2 emissions (e.g. Reckien et al., 2006; Ribeiro et al., 2019; Zhang et al., 2019). For instance, fragmented cities release more CO_2 from the traffic sector than compact cities (Makido et al., 2012). The high-rise apartment building is a better choice in the build use stage as the single-family buildings lead to the enhance of CO_2

Table 2.1 An overview of urban carbon emission studies. * indicates the values do not include in the references. Bottom-up method estimates CO_2 emissions from different sectors via sub-models and emission inventories. Inventory method refers to summarizing all known CO_2 emissions and storages in study area. Inverse model calculates CO_2 emissions using the atmospheric transport model based on the inversion of observational atmospheric CO_2 concentrations. Boundary-layer budget method refers to calculating the CO_2 stored in the defined volume and the CO_2 exchange through the sides.

Reference	City	Measurement height (m)	Population density (people km^{-2})	Measurement method	Period	Annual net carbon flux ($kg\ C\ m^{-2}\ year^{-1}$)
Christen et al. (2011)	Vancouver, Canada	26	6420	eddy covariance bottom-up method	May 2008-Apr 2010	6.7 7.5
Järvi et al. (2012)	Helsinki, Finland	31/29	3050*	eddy covariance	Jan 2006-Dec 2010	1.8
Song et al. (2013)	Beijing, China	140	14000	eddy covariance bottom-up method	2009	8.8 8.9
Velasco et al. (2014)	Mexico City. Mexico	37	8038	eddy covariance	Jun 2011-Sep 2012	6.7
Ward et al. (2015)	London, UK	48.9	31000*	eddy covariance inventory method	2011-2012	12.7 13.0
Menzer and McFadden. (2017)	Saint Paul, USA	40	1000	eddy covariance	2007-2008	1.3
Sargent et al. (2018)	Boston, USA		5338*	inverse model	Sep 2013-Dec 2014	0.9
Björkegren and Grimmond. (2018)	London, UK		31000*	boundary-layer budget method inventory method	Jun 2012-May 2013	14.0 14.5

emissions per inhabitant (Pacheco-Torres et al., 2016). The compact design of the traffic system is important in urban CO_2 mitigation (Wang et al.2018).

2.3 Modelling of CO_2 flux

In general, CO_2 flux in urban region can be modelled by "bottom-up" and "top-down" methods (Bergamaschi et al., 2018). Within bottom-up method, CO_2 emissions form each source sector, such as people activities, traffic, buildings, and vegetation, are estimated individually, and thus, the carbon footprint of each object is revealed clearly (Christen et al. 2011). With this method, the detailed emission inventories for each emission sector are required. Top-down method always exploits atmospheric transport model to estimate the CO_2 flux via the inversion of observational atmospheric CO_2 concentrations. The basis of the atmospheric inversion is the initial CO_2 flux. The uncertainties of the top-down method can be traced to the errors of observations, the prior CO_2 flux, and the atmospheric transport model (Feng et al., 2016). For example, based on the biogenic CO_2 flux data from satellites and input CO_2 fields as initialization and lateral boundary conditions, Ahmadov et al. (2009) exploited the Weather Research and Forecasting (WRF) model to simulate the time series of CO_2 concentration at a coastal station and interpret the impacts of mesoscale transport on CO_2 distribution.

In this study, the bottom-up approach is utilized and the CO_2 fluxes from different sources are simulated separately in the model.

2.3.1 Anthropogenic components

The urban anthropogenic CO_2 sources includes industrial activities, traffic, human metabolism, and building heating and energy production. Emissions from industrial activity or power plants always take place away from the urban region or beyond the study layer. Therefore, at the neighborhood scale where this study also focuses, traffic, domestic building heating and human metabolism are the most relevant anthropogenic sources.

Nejadkoorki et al. (2008) modelled the urban CO_2 emission from road traffic in street level by taking into account the road traffic characteristics such as vehicle type and speed, traffic flow and travelled distance. The total CO_2 emission (E_{TC}, g) for a given vehicle type v in the study area is defined as

$$E_{TC} = \sum_1^N F_{sv} \times D_{sv} \times C_{sv}, \quad (2.1)$$

where N is the amount of street segments, F_{sv} is traffic flow on a segment of road, D_{sv} (km) is the travelled distance on a segment, and C_{sv} (g km^{-1}) is the CO_2 emission factor on a road segment for the given vehicle type v.

Christen et al. (2011) exploited two separate building energy models for residential buildings and commercial buildings in bottom-up method to estimate the CO_2 emissions from building sector. The input of the building energy models also involves building attributes from LiDAR (Light Detection and Ranging) and house audits. For human metabolism estimation, they simply used the nocturnal population distribution multiplied by typical respiration value of a human body.

2.3.2 Biogenic components

The net ecosystem exchange (NEE) of CO_2 can be expressed as the balance between the gross primary production (GPP) and the ecosystem respiration.

Light-response curve approaches are always implemented to estimate the response of CO_2 flux to the light level as it affects the ecosystem photosynthesis (Bergeron and Strachan, 2011; Lasslop et al., 2012). The function can be established using a rectangular hyperbolic form:

$$NEE = -\frac{\alpha\beta R_g}{\alpha R_g + \beta} + \gamma, \quad (2.2)$$

where α (μmol CO_2 photons^{-1}) is the mean apparent light use efficiency, which indicates the initial slope of the light–response curve, β (μmol CO_2 m^{-2} s^{-1}) is the light-saturated CO_2 uptake rate, R_g (W m^{-2}) is the global radiation, and γ (μmol CO_2 m^{-2} s^{-1}) refers to the ecosystem respiration. Lasslop et al. (2012) modified the common rectangular hyperbolic light-response curve by replacing the constant respiration with a temperature dependence model of respiration and involving the vapor pressure deficit (VPD) dependency. Their work improved the model ability to perform the asymmetric diurnal cycle of CO_2 flux during high VPD period and enhanced the reliability of model results.

Ögren et al. (1993) suggested that the non-rectangular hyperbola equation could be a better way to describe the light-response curve. According to this, Bellucco et al. (2017) developed a non-rectangular hyperbola (NRH) method to improve the light-response curve and simulate the CO_2 uptake by photosynthesis ($F_{CO_2,pho}$, μmol CO_2 m^{-2} s^{-1}), which can be expressed as

$$F_{CO_2,pho}(R_g, \lambda_v, LAI) = -\frac{1}{2\theta(\lambda_v)}\left\{\alpha PAR + \beta(LAI, \lambda_v) - \left[\left(\alpha PAR + \beta(LAI, \lambda_v)\right)^2 - 4\alpha\beta(LAI, \lambda_v)\theta(\lambda_v)PAR\right]\right\}, \quad (2.3)$$

where λ_v is the vegetation cover fraction, LAI ($m^2\ m^{-2}$) is the leaf area index, θ is the convexity of light saturated curve, PAR ($W\ m^{-2}$) is the photosynthetically active radiation that can be used by leaves for photosysthesis, and other symbols have the same definition with Equation 2.2. The evaluation of model in suburban region of Helsinki suggested that it performed well during daytime, but systematically underestimated CO_2 emissions at nighttime.

Mäkelä et al. (2008) exploited the light use efficiency (LUE) approach to simulate daily GPP of the canopy empirically. The LUE type model estimated the conversion of radiation to GPP by introducing the LUE and modifying factors, which is defined as

$$F_{CO_2,pho} = c\Phi_k f_L(\Phi_k) f_T(\mathrm{T}_k) f_D(\mathrm{D}_k) f_\theta(\theta_k), \quad (2.4)$$

where c (g C mol^{-1}) is the potential daily LUE, Φ_k (mol m^{-2}) is the daily absorbed photosynthetically active radiation (APAR) during day k , and f refers to different modifying factors in day k. f_L, f_S, f_D, and f_W are responses of photosynthesis to the APAR, the mean daily ambient temperature (T), the vapour pressure deficit (D), and the soil water content (θ), respectively. The validation with eddy covariance data in several European sites indicated that the LUE model worked well with the APAR, temperature, and VPD modifiers. The geographical heterogeneity should be considered so that the potential LUE and the modifiers needed to be estimated in specific site.

Mäkelä et al. (2006) utilized an Arrhenius-type exponential equation of soil temperature to model the total ecosystem respiration. To simplify the input data of the bottom-up model at hand, the soil and vegetation respiration $F_{CO_2,\mathrm{res}}$ ($\mu mol \cdot m^{-2} \cdot s^{-1}$) can be simulated as the exponential function of air temperature (T_{air}, ℃) (Bellucco et al., 2017):

$$F_{CO_2,\mathrm{res}} = a \cdot exp(b \cdot T_{air}). \quad (2.5)$$

Here, a and b are the empirical site-specific constants. Bellucco et al. (2007) pointed out that the difference between the observed respiration and model respiration from temperature driven equation could be accepted.

3 Material and methods

3.1 Study area

Jätkäsaari is a peninsula and located at the southwest of central Helsinki (Figure 3.1). It used to be the main cargo port of Helsinki before late 2008, and until now, the Länsisatama harbour in the southwestern part remains a lively passenger port. Residential and commercial buildings were concentrated in the north and northeast Jätkäsaari along the access roads to city center, while a majority of the area was wasteland.

Jätkäsaari is planned to be built as a modern urban district and western extension to Helsinki City Center. The construction of this new maritime inner city district commenced in 2009, and the first project was the bridge connecting it to Ruoholahti. Residential construction began in 2011. By 2030, Jätkäsaari is esitimated to have 18000 residents and offers about 6000 jobs (Uutta Helsinkiä, 2019). Compact city blocks, as well as new traffic networks including tram, sidewalks and cycle routes, will be achieved based on the city plans (Helsinki City Planning Department, 2009).

Considering the distinct changes in urban appearance and functionality, Jätkäsaari is an ideal region to study the impacts of urban planning choices on CO_2 emissions and surface heat fluxes. In this paper, I selected the Jätkäsaari region of 1650 × 1400 m to model and compare the CO_2 emissions in past (2008) and future (2030) Jätkäsaari.

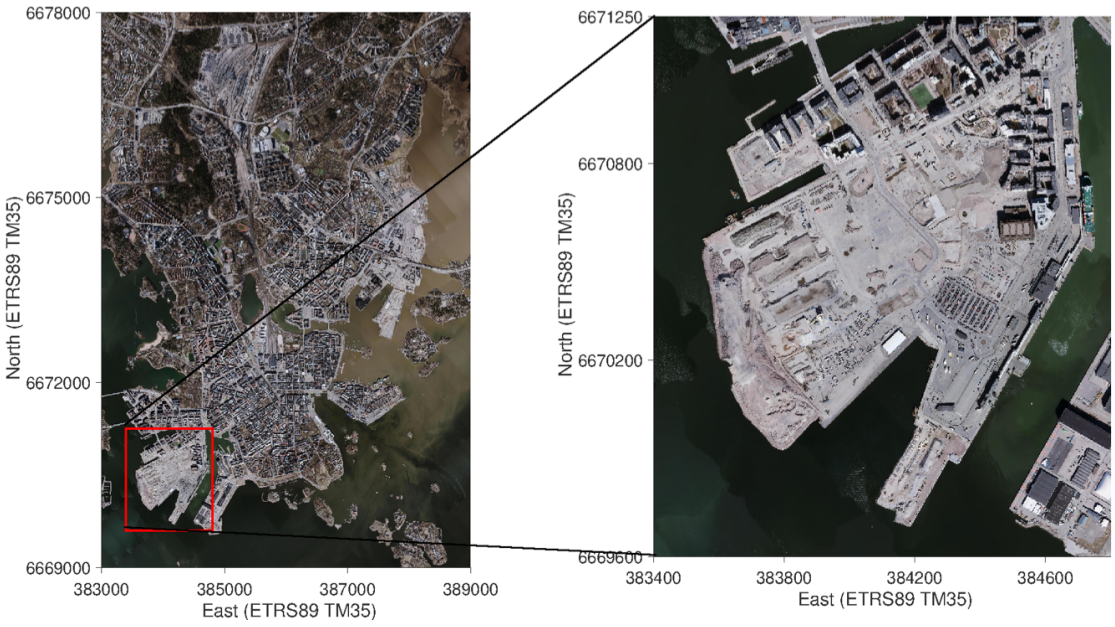

Figure 3.1 Orthoimagery of Helsinki and Jätkäsaari in 2014. (Projected coordinate system: ETRS89 TM35FIN) (City of Helsinki, kaupunkimittauspalvelut, 2014)

3.2 Model discription

3.2.1 Surface Urban Energy and Water balance Scheme (SUEWS)

The Surface Urban Energy and Water balance Scheme (SUEWS; Järvi et al., 2011) can be utilized to simulate the urban radiation, energy and water cycles, and CO_2 surface exchange on a local or neighbourhood scale.

The fundamental of SUEWS is the surface urban energy balance (Oke, 1987)

$$Q^* + Q_F = Q_H + Q_E + \Delta Q_S, \tag{3.1}$$

where Q^* is the net all-wave radiation, Q_F is the anthropogenic heat flux, Q_H is the sensible heat flux, Q_E is the latent heat flux, and ΔQ_S is the net storage heat flux.

On the basis of energy balance and the urban evaporation-interception approach (Grimmond and Oke, 1991), sub-models have been incorporated to minimize the number of required input variables and simulate more detailed urban energy and water exchange processes. The net all-wave radiation parameterization scheme (NARP) (Offerle et al., 2003) is able to calculate Q^* using the incoming shortwave radiation, relative humidity and air temperature. The Objective Hysteresis Model (OHM) (Grimmond and Oke, 1991) can calculate ΔQ_S. The local-scale urban parameterization scheme (LUMPS) (Grimmond and Oke, 2002) estimates Q_H and Q_E for the initial of atmospheric stability functions. Output Q_E is calculated with a modified Penman-Monteith equation for urban regions (Grimmond & Oke, 1991). Q_F is estimated considering the energy used for heating in cool temperature and cooling in warm temperature based on the heating and cooling degree-days, respectively (Järvi et al., 2011). Moreover, Q_H is calculated as the residual from the other energy balance components in Equation 3.1.

Particularly for urban regions, SUEWS considers seven different surface types: buildings, paved surfaces, evergreen trees and shrubs, deciduous trees and shrubs, grass, bare soil, and water (Figure 3.2). There is a single soil layer beneath each surface type. Information of different surface types such as proportions of each surface type, building and tree heights, albedo, emissivity, and moisture storage capacity should be provided as model inputs (Ward et al., 2016). The model also needs observational variables, such as wind speed, relative humidity, air temperature, pressure, precipitation (P) and shortwave radiation as meteorological forcing. In addition, SUEWS has been also developed for cold climate cities to include snow cover (Järvi et al., 2014).

SUEWS now can use the time-step of 30, 40 or 60 minutes for the energy balance, while it runs at a shorter time-step of 1-10 minutes for the water balance. 5 minutes is strongly recommended. With changes in surface characteristics and meteorological forcing, it can be run for several days to years.

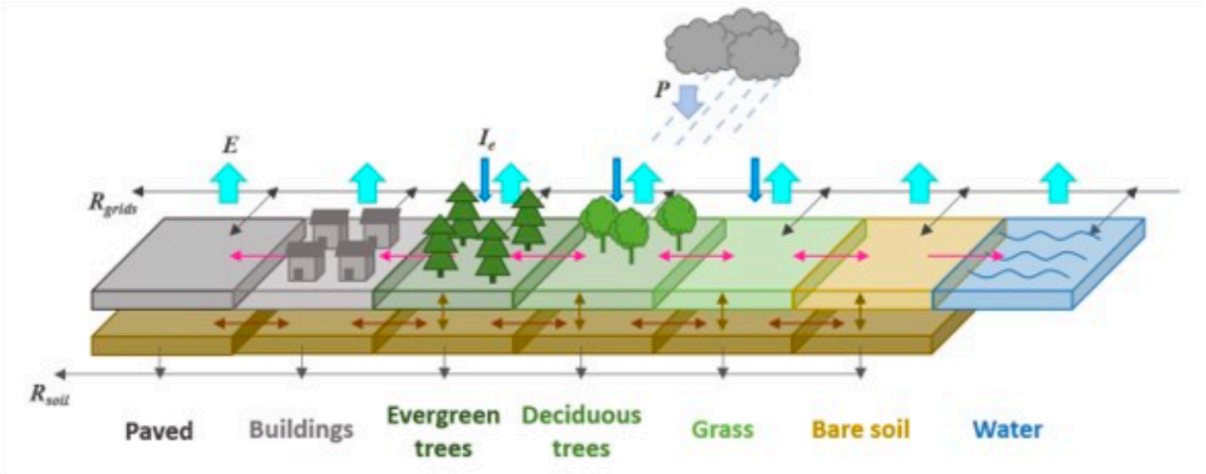

Figure 3.2. The seven surface types and water cycle in SUEWS. E is the evaporation, P is the precipitation, I_e is the external water supply, R_{grid} is the runoff between grids, and R_{soil} is the runoff in soil layer (SUEWS Documentation, Release v2018c).

3.2.2 CO_2 exchange module

A new module has been added into SUEWS to simulate both the urban anthropogenic and biogenic CO_2 emissions (Järvi et al. 2019). The anthropogenic local-scale CO_2 exchange (F_C, μmol m^{-2} s^{-1}) are separated into human metabolism (F_M), traffic (F_V), building energy and heating or cooling combustion (F_B), and point sources (F_P), while the biogenic CO_2 flux is the combination of CO_2 uptake by photosynthesis (F_{pho}) and CO_2 emissions from respiration (F_{res}). In this study, CO_2 exchange on water surfaces are not considered.

$$F_C = F_{C,ant} + F_{C,\,bio} = (F_M + F_V + F_B + F_P) + (F_{pho} + F_{res}) \quad (3.2)$$

The anthropogenic CO_2 emissions can be estimated by applying conversion factors to heat emission model (Sailor and Lu, 2004; Järvi et al., 2019).The hourly CO_2 emissions from human metabolism ($F_{M,h,d}$, μmol m^{-2} s^{-1}) and traffic ($F_{V,h,d}$, μmol m^{-2} s^{-1}) can be calculated by:

$$F_{M,h,d} = p_{h,d} \cdot H_{a,h,d} \cdot C_M, \quad (3.3)$$

and

$$F_{V,h,d} = Tr_d \cdot H_{T,d} \cdot E_{c,d}, \tag{3.4}$$

where $p_{h,d}$ (cap ha^{-1}) is the population density at daytime, $H_{a,h,d}$ is the diurnal profiles for population and activities, and C_M (μmol CO_2 s^{-1}cap^{-1}) is the metabolic CO_2 emission factor, Tr_d (veh day^{-1} area^{-1}) is the daily traffic rate, $H_{T,d}$ is the diurnal traffic profile, and $E_{c,d}$ (kg km^{-1}veh^{-1}) is the traffic CO_2 emission factor. In addition, CO_2 emissions from buildings needed to be accounted for if fossil fuels are used for the heating/cooling and energy production.

For biogenic components, CO_2 emissions from cellular respiration of soil and vegetation is assumed to follow an exponential relation to air temperature provided by Bellucco et al. (2017). In the equation, the soil respiration in wintertime is limited. The carbon uptake by photosynthesis can be calculated by the empirical canopy-level photosynthesis model (Järvi et al., 2019) modified from the LUE approach (Mäkelä et al., 2008). The leaf area index (LAI) is involved to modulate seasonal change of emissions across the year, and the environmental modifiers is added to revise the potential photosynthesis ($F_{pho,max,i}$).

$$F_{pho} = \sum_i (f_i F_{pho,max,i}) \mathrm{LAI}_i) f(T_{air}) f(\Delta q) f(\Delta\theta) f(K_{down}). \tag{3.5}$$

Here, the photosynthesis CO_2 sink (F_{pho}, μmol m^{-2} s^{-1}) is the sum of the product of potential photosynthesis, leaf area index, and surface fraction f_i over different vegetation surfaces i modified by the index depending on air temperature (T_{air}, ℃), specific humidity deficit (Δq, kg kg^{-1}), soil moisture deficit ($\Delta\theta$, mm), and incoming shortwave radiation (K_{down}, W m^{-2}). These indexes indicate the responses of photosynthesis to different environmental variables and can be estimated by observations.

3.2.3 Model evaluation

SUEWS has shown a good performance in urban energy and water cycles simulations by evaluating with measured surface heat fluxes and hydrological observations in several cities. In Vancouver, Canada, measured and modeled hourly net all-wave radiation, sensible heat flux and latent heat flux were in good agreement. The net all-wave radiation got the best estimation among them (Järvi et al., 2011). In Swindon, UK, SUEWS simulated the sensible and latent heat flux well. The r square of modeled and observed Q_H and Q_E reached 0.72 and 0.79, respectively (Ward et al., 2016).

The anthropogenic and biogenic CO_2 simulations were evaluated using EC observations from two sites: Kumpula and Torni, located at the semi-urban and city center of Helsinki, respectively (Järvi et al., 2019). The diurnal behaviors, as well as the annual values of carbon dioxide flux were well simulated. The modeled annual carbon emissions in the Torni site is 4640 g C m^{-2} $year^{-1}$, which is a little higher than the observation of 4507 g C m^{-2} $year^{-1}$. The root-mean-square deviation of modeled diurnal variation ranged from 0.06 μmol m^{-2} s^{-1} to 0.11 μmol m^{-2} s^{-1}. However, due to the lack of dynamic variations of traffic and population, the model cannot correctly or simultaneously simulate the peaks of CO_2 emissions.

Unfortunately, there was no observational surface flux data in our study areas. As Jätkäsaari is an extension part of Helsinki city center, SUEWS performance was assumed to be well and reliable similarly to the city center site.

3.3 Input data

Data used in SUEWS model runs as input in general can be obtained from different sources. In the following section, the description of the input meteorological data and site information is listed. The site specific surface information needed for each grid includes the area fractions of each surface type, building and vegetation heights, daytime and nocturnal population density, workday and weekend traffic rates.

3.3.1 Surface cover information

The land cover classification, as well as the building and vegetation heights in 2008 were determined with airborne lidar scanning data at 2 m resolution (Nordbo et al., 2015). The surface cover was classified into six types: buildings, impervious surfaces, grass, low vegetation or shrubs, high vegetation or trees and water. We assumed all low and high vegetations as deciduous in Jätkäsaari.

The surface cover information in 2030 was provided by the detailed urban planning map of Jätkäsaari (Helsinki City Planning Department, 2019). It was a three-dimensional urban model created by SketchUp including coloured surface and construction height. The surface types could be simply defined as buildings, paved surfaces, vegetation and water. To be consistent with the needed model input, the total vegetation areas were divided into grass (30%), shrubs (10%) and trees (60%), corresponding to the ratio of these three vegetation areas to total vegetation area in 2008.

Figure 3.3 compares the distribution of surface cover classes in Jätkäsaari in 2008 and 2030. Obviously, land reclamation along the coast, dense residential blocks, and green areas will have been constructed in the future. Note that when the future city plan map was transformed to surface cover, the area of paved surfaces would be slightly overestimated as the outlines of different surface types were distinguished as paved roads. The surface cover fractions in the whole study region were illustrated via pie chart in Figure 3.4. The pavement fraction increased from 32.6% to 37.2% in 2030. The fractions of building and vegetation areas changed little.

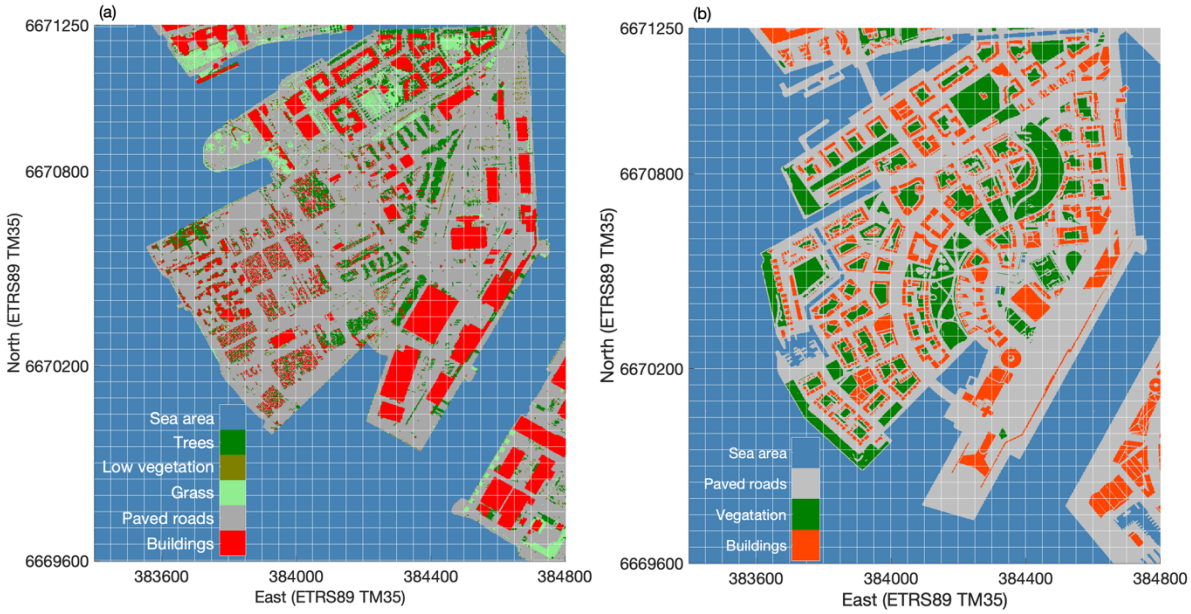

Figure 3.3 Surface cover classes in Jätkäsaari with 50 m × 50 m grids in (a) 2008, and (b) 2030.

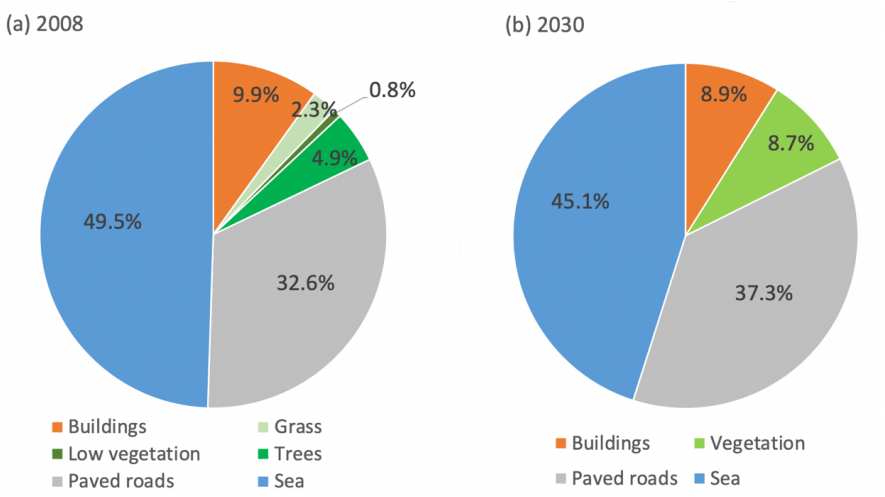

Figure 3.4 The fraction of different surface cover classes in Jätkäsaari in (a) 2008 and (b) 2030.

Figure 3.5 shows building and vegetation height in Jätkäsaari in 2008 and 2030. The vegetation height in 2030 was assumed to be equal to the average vegetation height of 7.8 m in 2008.

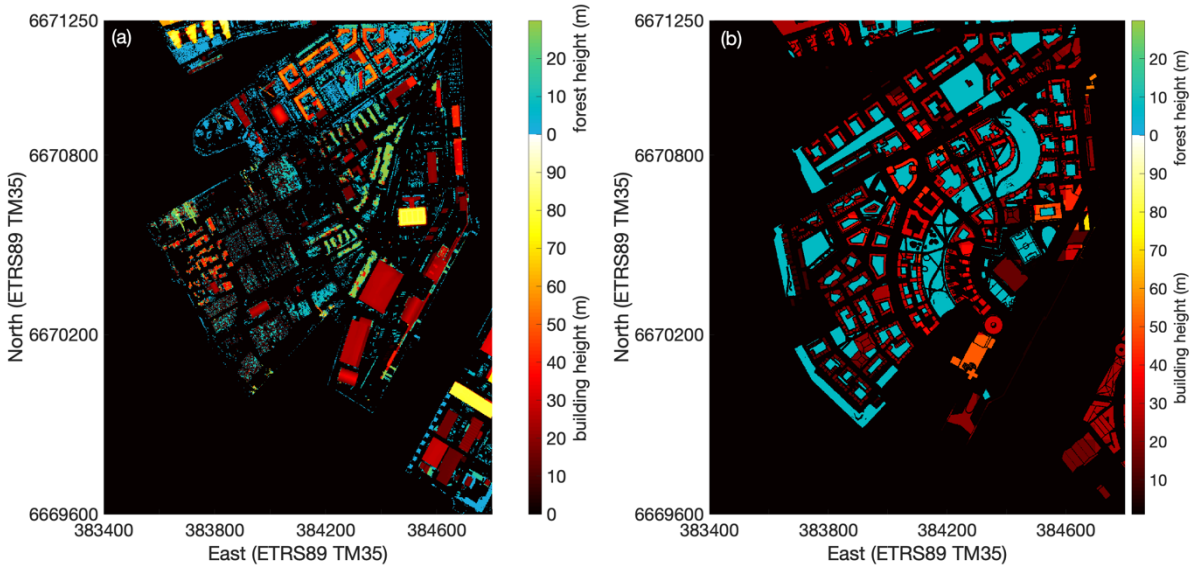

Figure 3.5 Building and vegetation height in Jätkäsaari in (a) 2008, and (b) 2030.

3.3.2 Population density

In SUEWS model, nighttime and daytime population is used to calculate anthrophonic CO_2 emissions from human metabolism. Nocturnal population data was obtained from SeutuCD building-level population database (HSY, 2011). The daytime population was estimated by the daily people work trip information from the Monitoring System of Urban Structure (YKR), produced by the Finnish Environment Institute and Statistics Finland (Järvi et al. 2019). This dataset was provided in the 250 m × 250 m lattices, and it collected the elaborate work movement information, including the coordinates of living and working grids, as well as the amount of different work trips. For each grid, the difference between daytime and nighttime population is calculated by the amount of entering and leaving work trips. As the lattice of the work journey data was larger than that of this study, the entering and leaving population was interpolated to grids which contain buildings according to the surface cover classes. Population density was expressed as the sum of building-level population within each grid divided by the grid area.

Figure 3.6 shows the nighttime and daytime population density in Jätkäsaari in 2008. At nighttime, people were concentrated on the residential areas in the northern Jätkäsaari. At

daytime, population density in residential areas decreased because people left for work. Besides residential buildings, people appeared on the central part and along the east coast of Jätkäsaari. The total nocturnal population was about 2250, while the value of daytime increased to about 7750.

Jätkäsaari would be home to 18000 residents in 2030 (Uutta Helsinkiä, 2019). In the future case, the nocturnal total population in our study region was assumed to be 18000, and then was evenly distributed into grids with buildings. Moreover, we assumed the all of 6000 jobs would belong to the incoming population at daytime. Based on the ratio of total arriving and leaving population at daytime in Jätkäsaari in 2008, the leaving population in 2030 could be roughly estimated. Thus, the daytime population in 2030 could be calculated by uniformly distributing the arriving and leaving population into each building grid. Here, we neglected the differences between residential and office buildings and simplified the estimation of the work trip information in 2030, which would bring uncertainties to anthropogenic CO_2 emission during simulation.

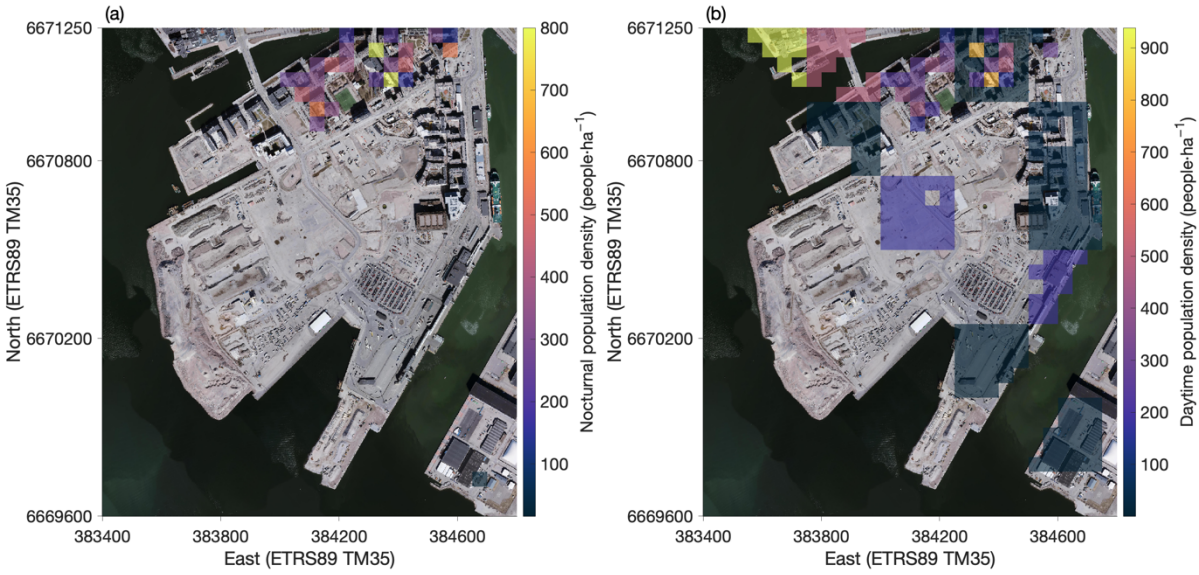

Figure 3.6 (a) Nighttime and (b) daytime population density (people ha-1) in Jätkäsaari in 2008.

3.3.3 Traffic rate

SUEWS model utilizes the traffic data to estimate the local-scale anthropogenic carbon emissions from traffic. Workday traffic volumes have been measured at different roads in Helsinki from 2007 to 2016 (Figure 3.7(a)). The weekend traffic rates were assumed as 77%

of the workday values (Kurppa et al., 2015). Traffic rate can be expressed as the total vehicle travelled distance per square meter per day. The vehicle travelled distance for each grid was approximately estimated by the product of the road length in each grid and the corresponding traffic volume. All of the traffic volumes were supposed to be measured in 2008 in order to obtain the spatial distribution of workday traffic rates (Figure 3.8). The traffic rate was around 0.18 veh km m^{-2} day^{-1} on the road connecting Jätkäsaari to Helsinki city center. On other roads of Jätkäsaari, the traffic rates were less than 0.1 veh km m^{-2} day^{-1}.

In the blueprint of future Jätkäsaari (Helsinki City Planning Department, 2008), the maximum of traffic volumes on major roads was predicted (Figure 3.7(b)) up to 30000 veh day^{-1} in 2030. The traffic volumes would gradually increase with construction. According to the traffic forecast (Helsinki City Planning Department, 2008), in 2009, the traffic volume from Jätkäsaari to Mechelininkatu was about 2,000 passenger cars daily, while this value would increase to 20000 passenger cars daily by 2030. What's more, there would be a loop-like tram network in future Jätkäsaari. A comprehensive and safe cycling and pedestrian network would be created in the future.

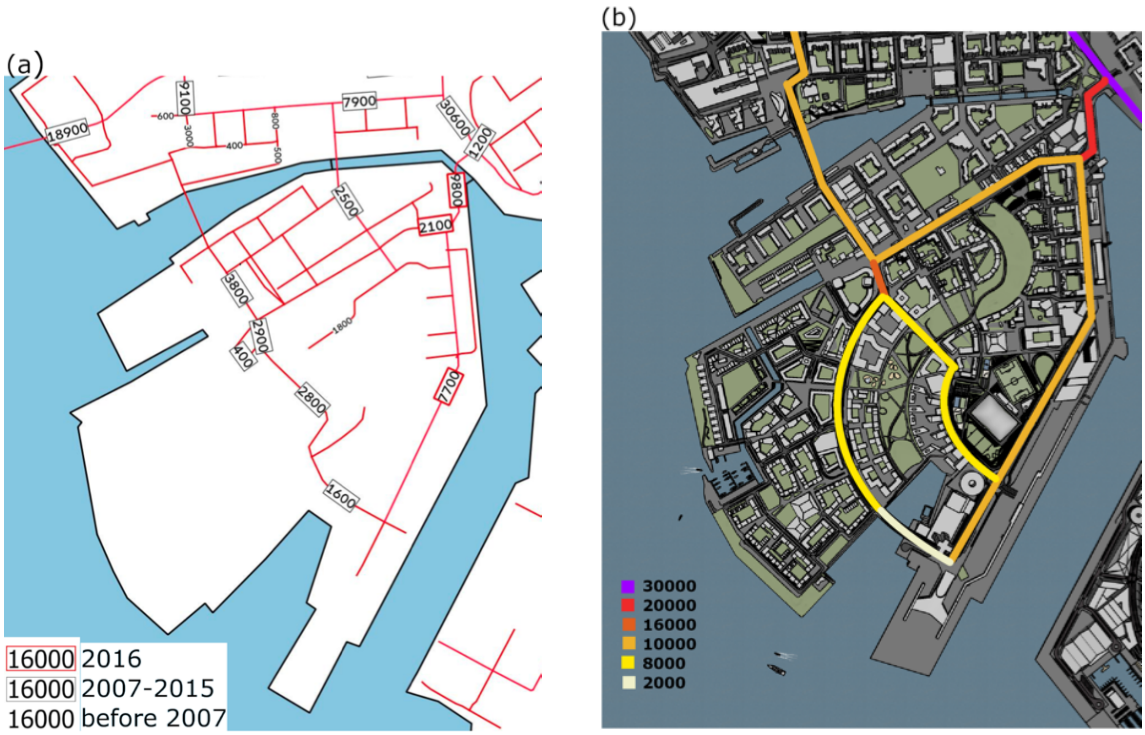

Figure 3.7. (a) Autumn workday traffic volume (veh day^{-1}) (HEL, 2017). The border types refer to measurement years. (b) Forecast traffic volumes (veh day^{-1}) in Jätkäsaari (Helsinki City Planning Department, 2008). Colour lines are major access roads with different traffic volumes.

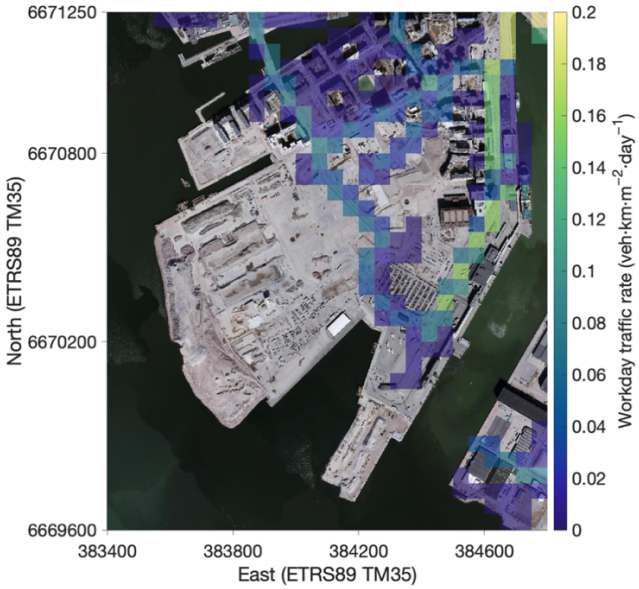

Figure 3.8 The spatial distribution of workday traffic rates (veh km m^{-2} day^{-1}) in Jätkäsaari in 2008.

3.3.4 Meteorological data

The meteorological forcing data combined the weather observations including wind speed, relative humidity, air temperature, pressure and precipitation at Kaisaniemi, Helsinki and the radiation observations of incoming shortwave radiation at Kumpula, Helsinki. All of the observational data were obtained from Finnish Meteorological Institute website (https://en.ilmatieteenlaitos.fi/download-observations#!/). The period was two years from January 2007 to December 2008 and time resolution was one hour. For the future case in 2029-2030, the same meteorological forcing data between 2007 and 2008 was exploited. We neglected the impacts of climate change and focused on the how the urban planning choices affect the future CO_2 emissions.

3.4 Model runs

3.4.1 Parameters used in SUEWS

Parameters used in SUEWS related to CO_2 emissions are listed in Table 3.1. To simulate the anthropogenic CO_2 emissions from traffic, the traffic emission factors for CO_2 needed to be estimated by the distribution of vehicles types and their corresponding emission factors. In this study, the CO_2 traffic emission factors for workdays and weekdays were set as 0.285 kg km^{-1} (Järvi et al., 2019).

Diurnal profiles of human activity, traffic, and population are shown in Figure 3.9, which are applied for converting the daily anthropogenic CO_2 emissions to daily ones. Additionally, In model version 2018c, the carbon sink, waterbody, was not considered and assumed to be zero. The fraction of fossil fuels used for building heating and energy production within the study area was set to be zero. There were no power plants or industries in the study domain. The CO_2 fluxes related to waterbody, buildings and point sources were not included in the model runs.

Table 3.1 Parameters in SUEWS related to CO_2 emission simulation.

Variable	Notation	Value	Unit	Reference
C_M	CO_2 release per capita	min: 120 max:180	μmol CO_2 $s^{-1}cap^{-1}$	Ward et al. (2013) Moriwaki and Kanda (2004)
$E_{c,d}$	CO_2 release per vehicle per meter of travel	0.285	$kg \cdot km^{-1}$	Järvi et al. (2012)
$F_{irr,veg}$	Fraction of irrigated vegetation	0.3		this study
$a_{decidtr}$	Empirical parameter in the relation of soil and vegetation respiration and air temperature	0.519		Järvi et al. 2019
$b_{decidtr}$		2.1		
a_{grass}		0.09		
$b_{decidtr}$		0.06		

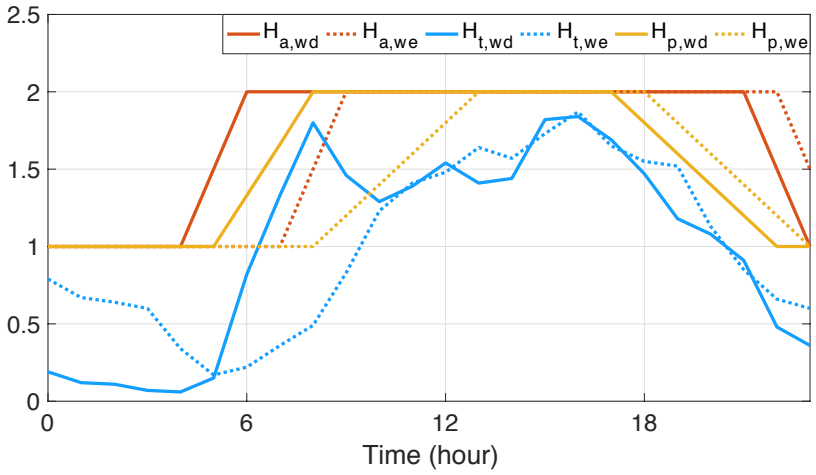

Figure 3.9 Diurnal profiles of human activity (H_a), traffic (H_t), and population (H_p) on workdays and weekends.

3.4.2 Experiment design

We conducted two experiments: one was to model the CO_2 emissions in Jätkäsaari in 2008 and the other was to model the CO_2 emissions in Jätkäsaari in 2030 when the construction of the area is estimated to be completed. The model was run in spatial resolution of 50 m × 50 m and time resolution of an hour in the 1650 m × 1400 m domain to simulate the CO_2 emissions and surface energy fluxes in each grid. There are 924 grids in total. The surface characteristics of each grid were given by data mentioned before. The same meteorological forcing was used for all grids on both simulated years: 2007-2008 and 2029-2030. The first year is the spin-up period of the model in order to remove its dependency on the initial values while the latter year was used in the actual analysis. The hourly output variables of 2008 and 2030 were used for the actual analyses.

4 Results and discussion

This chapter presents modelled results of total CO_2 emissions from anthropogenic and natural sources, and the spatiotemporal variation of urban CO_2 fluxes in selected Jätkäsaari region. Through the comparison between the modelling output of previous and future case, the influences of urban planning on CO_2 emissions in Jätkäsaari are analyzed in detail. The model uncertainty on CO_2 simulation is also discussed. Hereafter, CO_2 emission sources only include road traffic, human metabolism, respiration of vegetation and soil, and the CO_2 sink refers to vegetation photosynthesis. The positive CO_2 fluxes indicate the CO_2 sources, while the negative ones indicate the CO_2 sink. Note that in this study, the mass of CO_2 is estimated so that the units are always kg CO_2 m^{-2} $year^{-1}$ or kt CO_2 year-1, which are different from the units in some other references that only measuring the mass of carbon.

4.1 Total areal CO_2 emissions

In 2008, the modelled total CO_2 discharged into the atmosphere in Jätkäsaari is 3.0 kt CO_2 $year^{-1}$ (Fig. 4.1). The largest two emission sources are human metabolism and road traffic, both of which emit 1.9 kt CO_2 per year. The emission from soil and vegetation respiration is 0.5 kt CO_2 $year^{-1}$, while the CO_2 uptake of plant photosynthesis is 1.3 kt CO_2 $year^{-1}$ resulting in a net ecosystem sink of -0.8 kt CO_2 $year^{-1}$. The contribution of different sources on total CO_2 emission is 44% for metabolism, 44% for traffic, and 12% for respiration.

In 2030, the total CO2 emission in study area is 11.1 kt CO_2 $year^{-1}$. The three source sectors emit 12.5 kt CO_2 per year, of which 6.6 kt (53%) originates from traffic, 5.3 kt (42%) comes from metabolism, and 0.6 kt (5%) originates from the respiration of vegetation and soil. The only sink, vegetation, absorbs 1.4 kt CO_2 $year^{-1}$and the NEE equals to -0.8 kt CO_2 $year^{-1}$.

According to Järvi et al. (2019), in a 6 × 9 km^2 domain of Helsinki, the total carbon emissions were 81.8 kt in 2012, and dominated also by anthropogenic emissions involving traffic and human metabolism. The emissions related to buildings are only 0.003 kt C $year^{-1}$. However, in the large area of Helsinki, the vegetation acts as a source in total, which is different from Jätkäsaari. In a 4 km^2 residential neighbourhood of south central Vancouver, Canada, the total amount of carbon released to the atmosphere estimated by a bottom-up model was 26.9 kt C $year^{-1}$ (Christen et al., 2011). The transportation contributed to 70% of the total emissions followed by the buildings. The human respiration only accounted for 5% of the total carbon emissions, which was much lower than that of Helsinki. The vegetation was modeled as a carbon sink. Velasco et al. (2014) partitioned the CO_2 fluxes and pointed out that vehicular

traffic contributed 72% to the local CO_2 emissions in Mexico City. In cities of Massachusetts, USA, the vegetation respiration released the equivalent of 11% of the anthropogenic CO_2 emissions, while photosynthesis absorbed the equivalent of 14% of that (Hardiman et al., 2017). Compared to the results of Jätkäsaari in 2008, the CO_2 emissions from respiration is the equivalent of 13% of the anthropogenic CO_2 emissions, while the CO_2 uptake by photosynthesis is the equivalent of 44% of that.

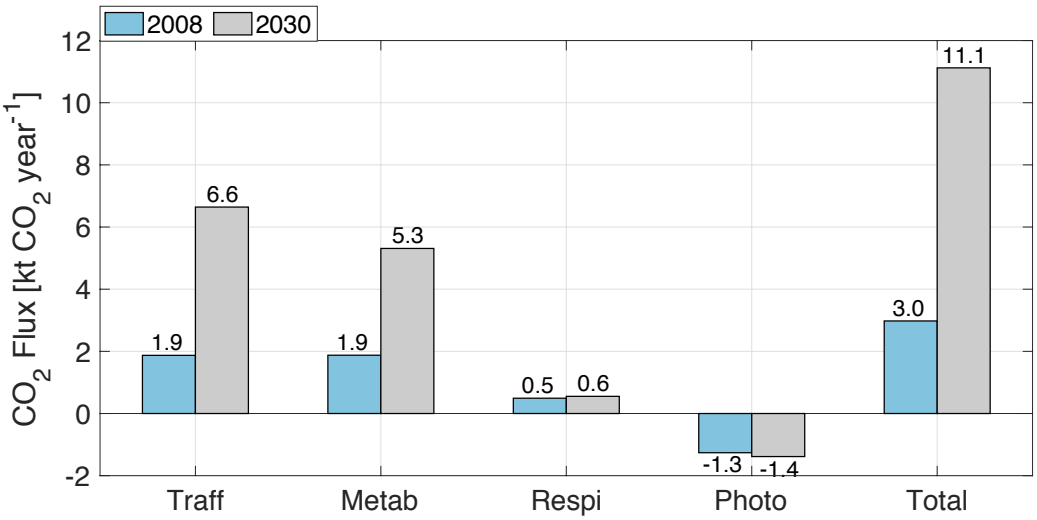

Figure 4.1 Cumulative CO_2 fluxes related to traffic, metabolism, respiration and photosynthesis, and total CO_2 emissions within Jätkäsaari in 2008 and 2030.

4.2 Spatial variability of urban CO_2 fluxes

4.2.1 Anthropogenic components

In the study region, the spatial distributions of annual cumulative CO_2 emissions from anthropogenic sources including road traffic and human metabolism have obvious variability due to the source distributions. No building emissions takes place due to no fossil fuel fraction in district heating mode. From raster maps in Figure 4.2, the metabolism CO_2 fluxes reflect the emissions from the combination of daytime and nighttime population density distributions. In 2008, the emission hotspots are at the residential area in northern Jätkäsaari with the values larger than 10.0 kg CO_2 m^{-2} $year^{-1}$. The maximum metabolism emission is 24.0 kg CO_2 m^{-2} $year^{-1}$. As there are approximate 15800 more people living and working in Jätkäsaari in 2030 than in 2008, and the residential and commercial buildings are distributed uniformly in 2030,

the metabolism emissions exist in almost all grids. The hotspots are located in the east of the study region with dense office buildings with a maximum emission of 23.6 kg CO_2 m^{-2} $year^{-1}$.

Both maps of annual traffic CO_2 emissions in 2008 and 2030 (Figure 4.3) reveals the large emissions in the major roads due to high traffic volumes. A large amount of CO_2 releases from relatively small areas in the total region. There are distinct hotspots in the access from Jätkäsaari to Hietalahti which is the major transport route from the Jätkäsaari harbor to city center. The high CO_2 emissons of this traffic route are 18 kg CO_2 m^{-2} $year^{-1}$in 2008 and 39 kg CO_2 m^{-2} $year^{-1}$in 2030.

The magnitude of the maximum metabolism emission in Jäkäsaari is similar to that in Helsinki city centre, where the maximum value was estimated as 9.1 kg C m^{-2} $year^{-1}$ (Järvi et al., 2019). Part of the difference is probably due to the model spatial resolution: 250 m in Järvi et al (2019) and 50 m in this study. In Vancouver, Canada, the average CO_2 emission from human respiration in a residential neighbourhood was modelled as 0.49 kg C m^{-2} $year^{-1}$ (Christen et al., 2011). The difference might come from the emission inventories used in the bottom-up model. The average CO_2 emission from transportation in south central Vancouver was estimated as 2.93 kg C m^{-2} $year^{-1}$ (Christen et al., 2011). In the west of Helsinki city centre, the value of annual traffic CO_2 emission is about 6.2 kg C m^{-2} $year^{-1}$ (Järvi et al., 2019). The annual anthropogenic emissions in the Boston urban region was reported as 0.9 kg C m^{-2} $year^{-1}$ by the inverse model (Sargent et al., 2018).

Uncertainties in modelling anthropogenic CO_2 emissions are possibly derived from the estimation of the population density, the traffic volumes, and the CO_2 emission factors related to human metabolism and traffic. The YKR dataset of work trips may overestimate the population in specific areas as it neglects the different locations of branches and the shift work (Järvi et al., 2019). Moreover, the lattices in TKR dataset are larger than those in our model domain. Errors may be introduced by interpolating it to grids with buildings. In this study, CO_2 release per vehicle per meter of travel is set to be same in 2008 and 2030. However, the proportion of vehicles with alternative driving power has increased from zero in 2007 to 7% in 2020 (Finnish Transport and Communications Agency, 2017). The trend of future vehicles indicates that there will be more passenger cars with alternative driving power such as electricity and plug-in hybrids so that the emission factors will change synchronously. Considering the linear relation of carbon emissions and emission factors, the difficulties in the estimation of emission factors resulted in the uncertainties of CO_2 traffic emissions.

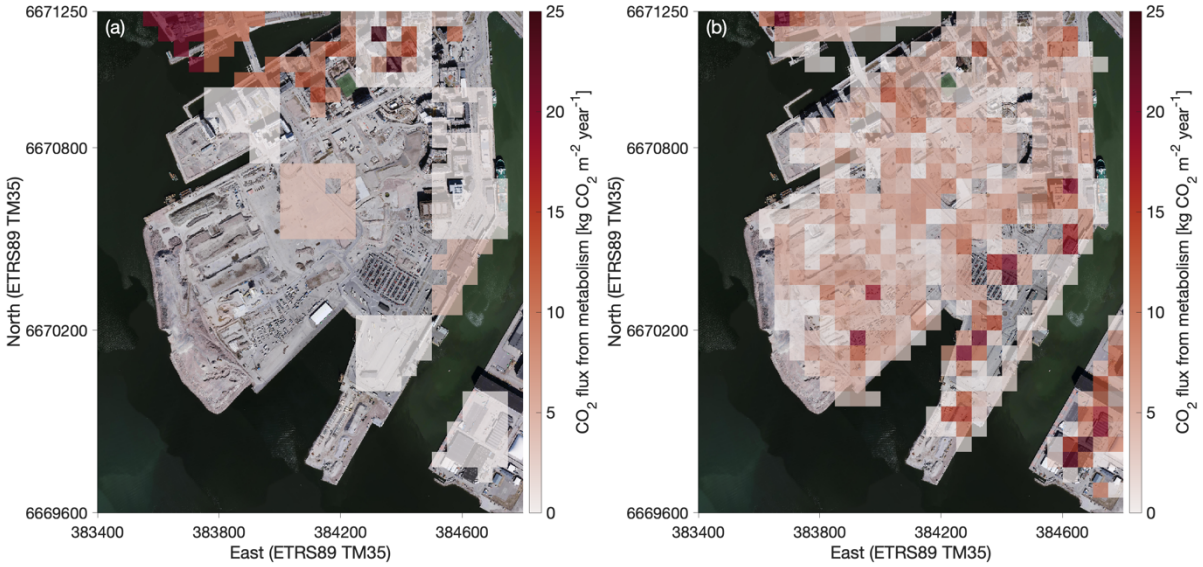

Figure 4.2 Raster maps of annual cumulative CO_2 emissions at 50 m grid resolution from human metabolism in Jätkäsaari in (a) 2008 and (b) 2030.

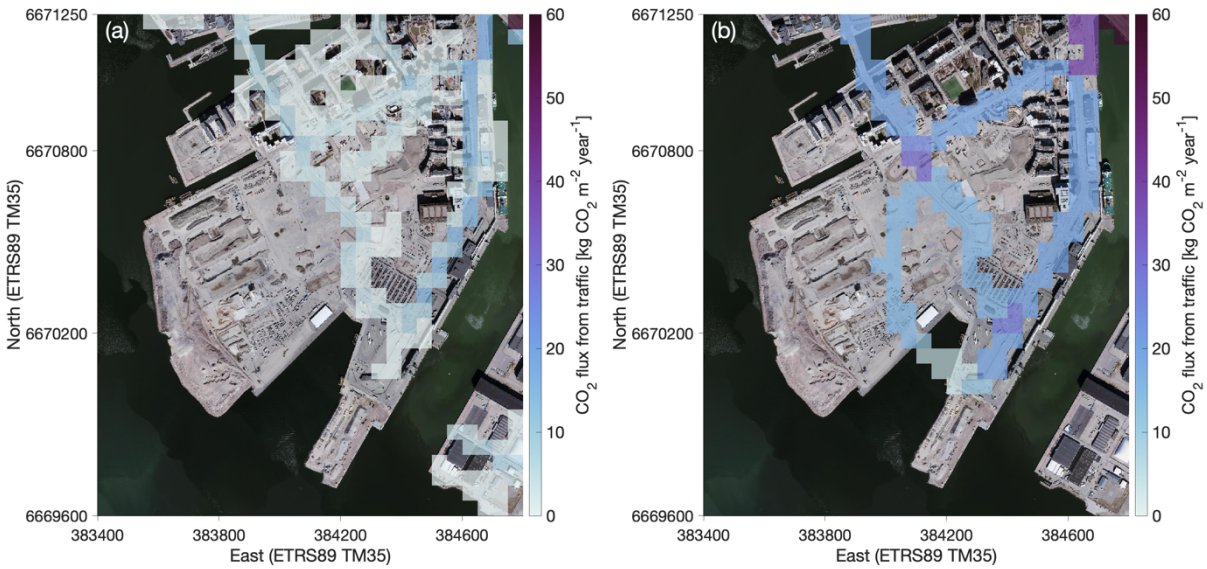

Figure 4.3 Raster maps of annual cumulative CO_2 emissions at 50 m grid resolution from road traffic in Jätkäsaari in (a) 2008 and (b) 2030.

4.2.2 Biogenic components

The distributions of annual total CO_2 emissions due to soil and vegetation respiration are shown in Figure 4.4. The high vegetated areas are obviously visible in the raster maps as the CO2 flux from respiration follows an approximate linear response to the vegetation fraction (see Figure 4.6a). Note that the range of CO_2 flux from respiration for the same vegetation fraction mainly comes from the proportion of different vegetation classes including grass, deciduous and evergreen vegetations with different soil respiration level. In 2008, the hotspots of CO_2 released by respiration are found in the north of Jätkäsaari, where the vegetation fraction exceeds 70%, with a maximum value of 3.2 kg CO_2 m^{-2} $year^{-1}$. In 2030, the hotspots of respiration CO_2 emissions are mainly located at two large green areas with CO_2 emissions over 2.5 kg CO_2 m^{-2} $year^{-1}$.

Figure 4.5 presents the modelled annual accumulative CO_2 sink by photosynthesis. The hotspots of CO_2 sink are found in the same locations as those of respiration CO_2 flux, where there are large green areas and parks. The CO_2 sink increases with the rising of vegetation fraction (Figure 4.6b). The range of CO_2 flux from photosynthesis results from the different fractions of vegetation classes. The maximum of CO_2 sink in the study region is -8.2 g CO_2 m^{-2} $year^{-1}$ in 2008 and -6.5 kg CO_2 m^{-2} $year^{-1}$ in 2030.

It is noteworthy that the biogenic CO_2 fluxes are an order of magnitude smaller than the anthropogenic CO_2 fluxes. The NEE can be calculated by the combination of CO_2 fluxes from respiration and photosynthesis. In this study, the annual total NEE is always negative in all vegetated grids (Figure 4.7). The CO_2 absorption by photosynthesis cancels out the CO_2 discharge of soil and vegetation respiration, and thus leads to the negative NEE, which is much lower in high vegetated areas. The minimum values of NEE in study areas reach -5.1 kg CO_2 m^{-2} $year^{-1}$in 2008 and -3.8 kg CO_2 m^{-2} $year^{-1}$in 2030. These results are in agreement with Järvi et al. (2019) results that the negative NEE appeared in the city centre of Helsinki as there were fewer organic matters for the respiration process. However, in the forest in northern Helsinki, the annual NEE was maintained positive and the forest played a role of CO_2 source probably due to the short growing season in the high latitude region. Uncertainties in simulating the net biogenic CO2 fluxes originate from both respiration emissions and photosynthesis uptake. Since it is the difference between these two values, small errors can lead to large uncertainties of NEE and affect the sign of NEE.

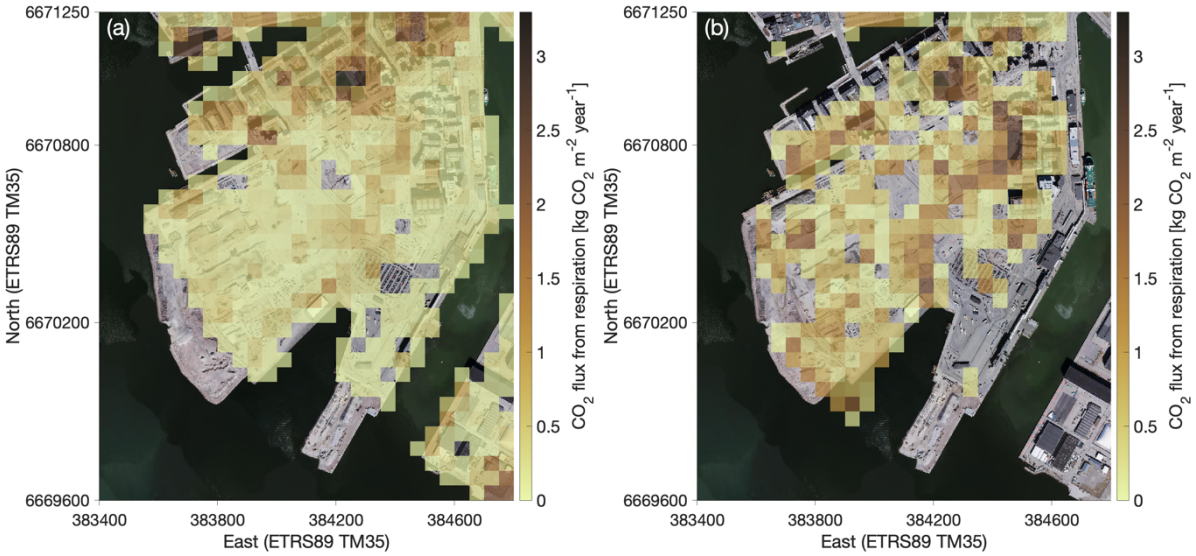

Figure 4.4 Raster maps of annual cumulative CO_2 emissions at 50 m grid resolution from soil and vegetation respiration in Jätkäsaari in (a) 2008 and (b) 2030.

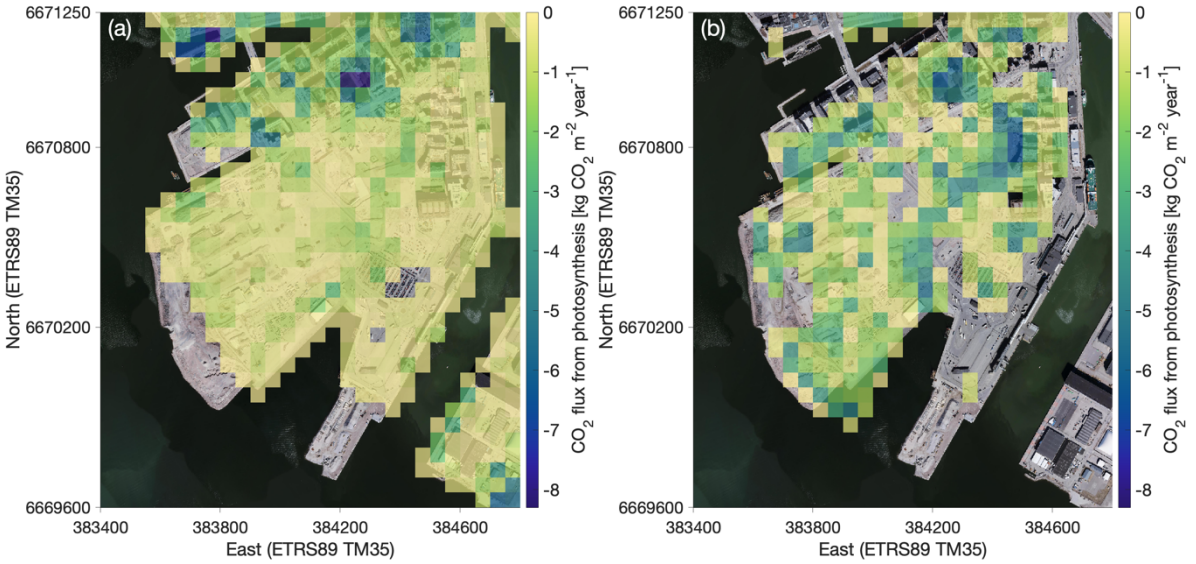

Figure 4.5 Raster maps of annual cumulative CO_2 uptake at 50 m grid resolution by vegetation photosynthesis in Jätkäsaari in (a) 2008 and (b) 2030.

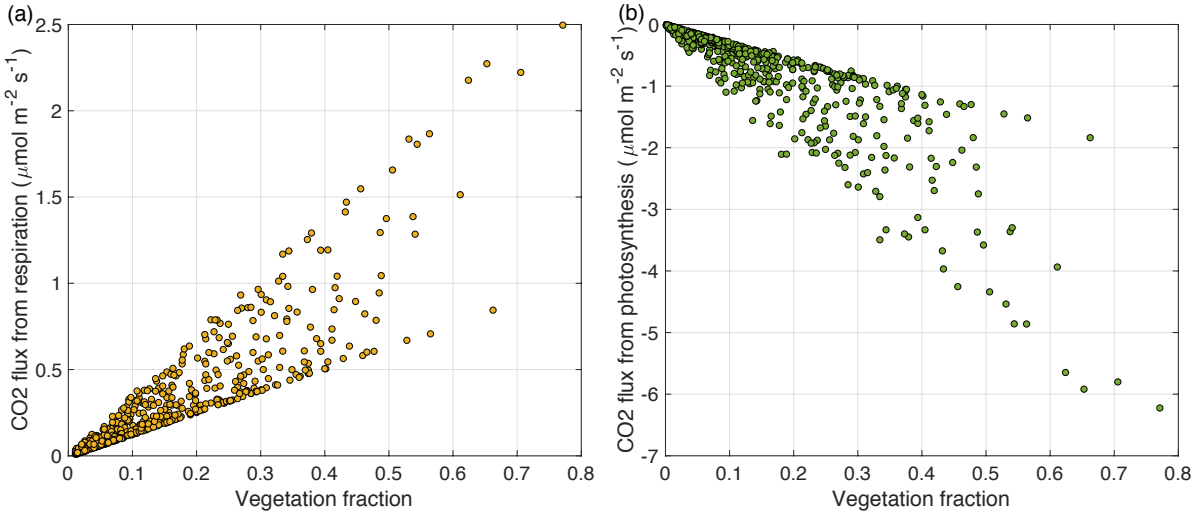

Figure 4.6 Relations between vegetation fraction and CO_2 fluxes from (a) respiration, and (b) photosynthesis.

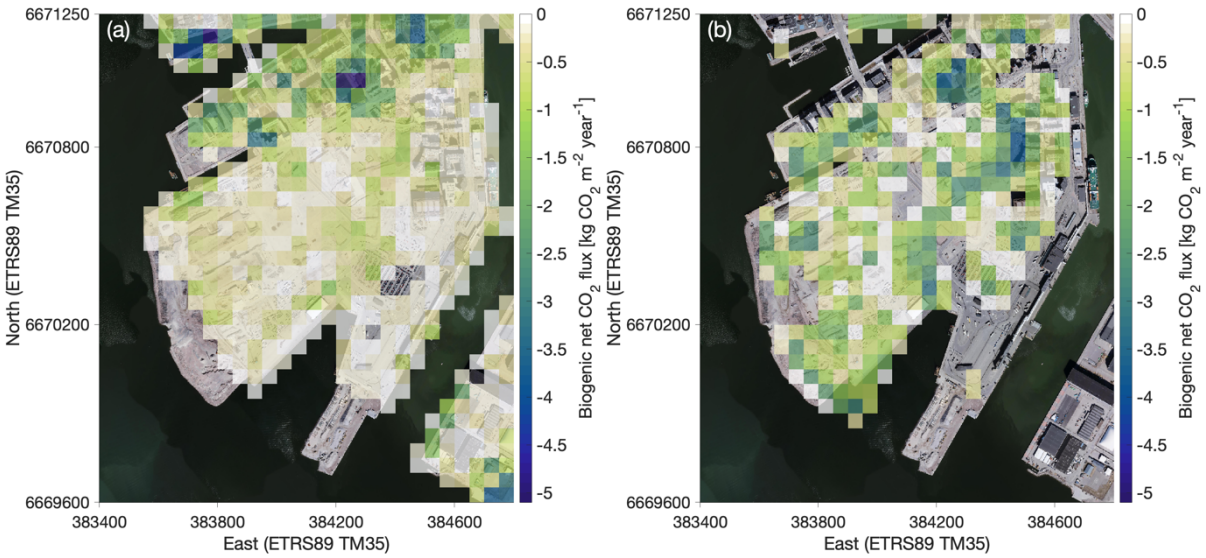

Figure 4.7 Raster maps of annual cumulative biogenic net CO_2 flux at 50 m grid resolution in Jätkäsaari in (a) 2008 and (b) 2030.

4.2.3 Integrated emissions

The spatial variability of net CO_2 flux is shown in Figure 4.8. In 2008, the annual total net CO_2 flux ranges from -5.1 kg CO_2 m^{-2} $year^{-1}$ to 29.5 kg CO_2 m^{-2} $year^{-1}$ except for the grids in the northeast corner outside of Jätkäsaari peninsula. Because of the numerous anthropogenic

emissions, the hotspots of CO_2 emissions correspond to the major roads and dense residential neighbourhoods and office regions. The net CO_2 fluxes are negative in majority of grids because of the small residential areas. Vegetated grids with no inhabitants and traffic volumes become the CO_2 sink areas. In 2030, the values range from -3.8 kg CO_2 m^{-2} $year^{-1}$ to 52.1 kg CO_2 m^{-2} $year^{-1}$. The hotspots of CO_2 emissions were concentrated in avenues. In residential neighbourhoods, the net CO_2 fluxes are always positive but lower than roads. The CO_2 sink areas only appear in greenspaces in parks and near the coast, where the grids have high vegetation fraction and extremely low population density and no traffic volumes.

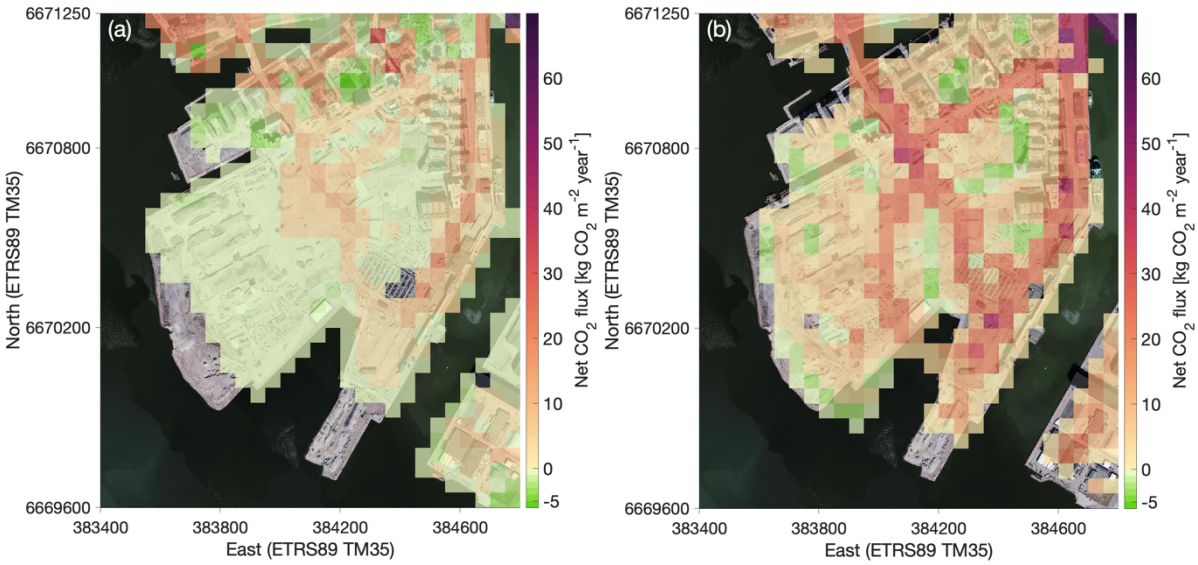

Figure 4.8 Raster maps of annual cumulative net CO_2 flux at 50 m grid resolution in Jätkäsaari in (a) 2008 and (b) 2030.

Figure 4.9 delineates the relative contribution of the three urban CO_2 emission sources for each 50 m lattice. In 2008, as the waste land occupies most of the area, vegetation is dominant sources except the arterial thoroughfare and residential and office buildings. In the green infrastructure along the street, both vegetation and traffic are major sources of urban CO_2 emissions. Although the grids with vegetated dominant emission are the majority, the vegetation respiration only takes up 12% of the annual total emissions. In 2030, human metabolism in construction areas dominates the CO_2 emissions in most grids with the exception of thoroughfare and parks. Only in very few grids near the coast and in the park with almost no traffic and population, the contribution of respiration to total CO_2 emissions is dominant.

Ward et al. (2015) reported that the enhanced CO_2 emissions were related to the reduced vegetation cover faction. The decreased vegetation areas not only indicated the decline of photosynthesis CO_2 sink, but also implied the increase of building and road areas which were associated with the anthropogenic emissions. In a neighbourhood with over 80% vegetation cover of Saint Paul, USA, the contribution of photosynthesis was largest among all CO_2 flux components during growing season. However, due to the balance of CO_2 fluxes form photosynthesis and respiration, the net biogenic flux was small so that the anthropogenic fluxes accounts more for the total neighbourhood emissions (Menzer and McFadden, 2017).

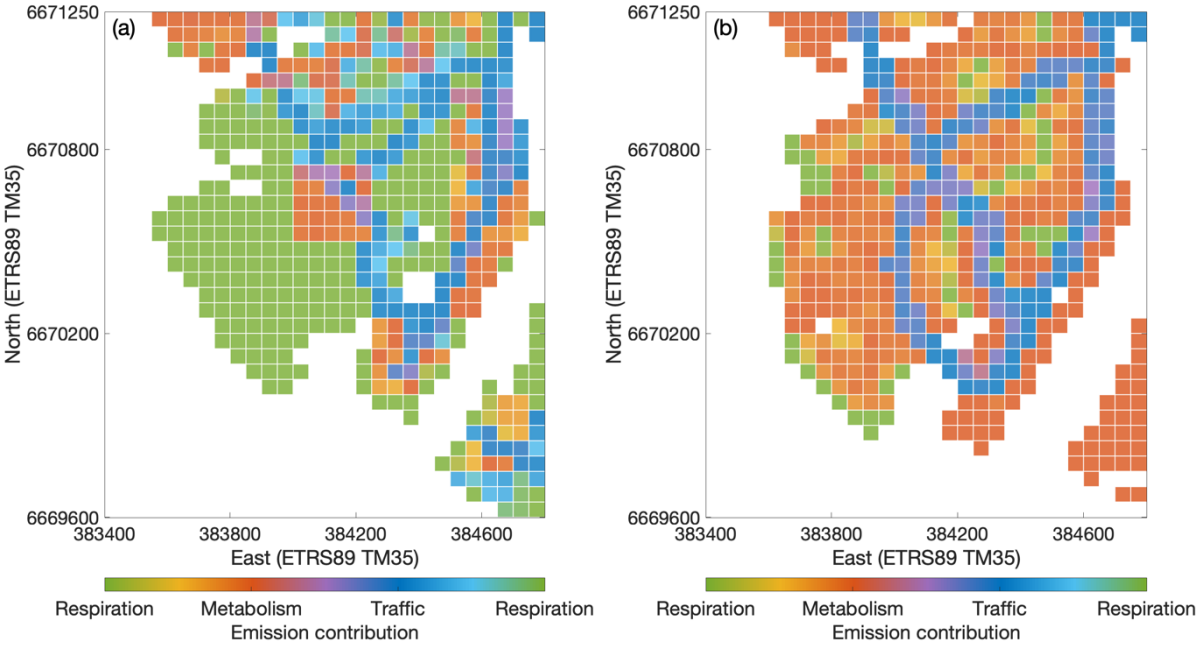

Figure 4.9 Relative contributions of CO_2 emission sectors: respiration (green), metabolism (red), traffic (blue) to the total emissions in Jätkäsaari in (a) 2008 and (b) 2030.

4.3 Monthly and seasonal variation

Table 4.1 illustrates the monthly variation of CO_2 fluxes from different sectors in Jätkäsaari in 2008 and 2030. In general, the anthropogenic (traffic and metabolism) emissions are stable on a monthly basis. The slight variation results in the different diurnal profiles of activity, traffic and population between workdays and weekends. The biogenic emissions reveal distinct seasonal variation due to the environmental factors, such as LAI, air temperature, soil moisture deficit, and the radiation. The CO_2 emission from respiration and the CO_2 uptake

from photosynthesis are both higher during summertime, while those are lower in wintertime. From April to September in 2008 and 2030, the CO_2 uptake by photosynthesis offsets the CO_2 release from respiration so that the NEE values are negative. Throughout the whole year, vegetation acts as a sink for CO_2 and reduces the CO_2 concentration in the atmosphere.

On a seasonal basis showed in Figure 4.10, in spring, autumn and winter, the net CO_2 emissions are maintained high values with slight seasonal differences. In summertime, the net CO_2 emissions are 1.0 g CO_2 m^{-2} day^{-1} in 2008 and 10.4 g CO_2 m^{-2} day^{-1} in 2030, which are much lower than values in other seasons. The net CO_2 emissions declines in summer period for the sake of intensive photosynthesis with strong shortwave radiation, increased LAI, as well as high temperature in that time.

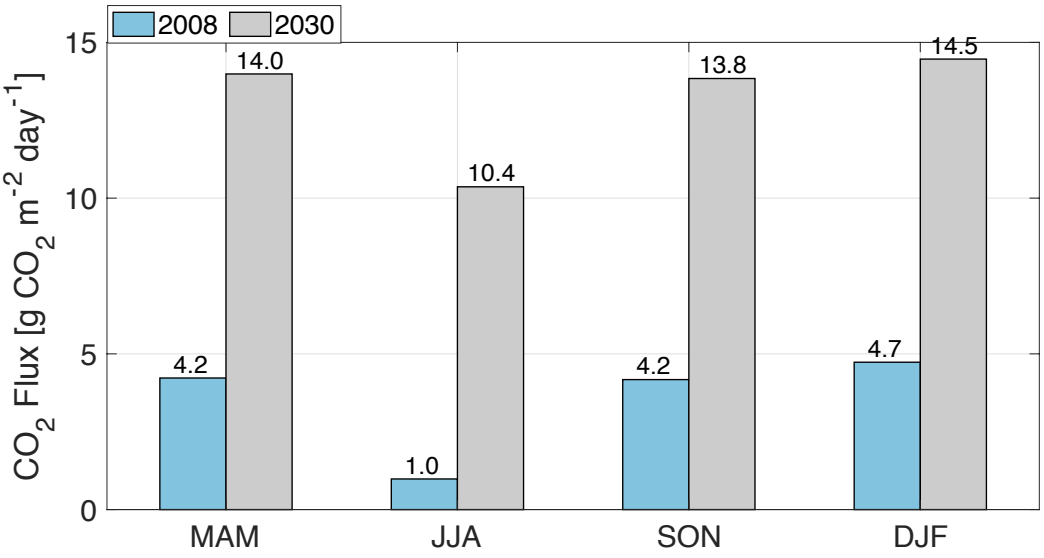

Figure 4.10 Seasonal CO_2 emissions from all sources in Jätkäsaari in (a) 2008 and (b) 2030. MAM, March to May; JJA: June to August; SON, September to November; DJF, December to February;

Table 4.1 Comparison of modelled CO_2 fluxes in 2008 and 2030 from different sources (traffic, human metabolism, vegetation respiration and photosynthesis) on a monthly basis in Jätkäsaari. (unit: g CO_2 m^{-2} day^{-1})

	2008						2030					
	Total	Traffic	Metab-olism	Rispira-tion	Photosy-nthesis	NEE	Total	Traffic	Metab-olism	Rispira-tion	Photosy-nthesis	NEE
Jan	4.8	2.2	2.2	0.3	0.0	0.3	14.5	7.9	6.3	0.4	0.0	0.3
Feb	4.6	2.2	2.2	0.3	-0.1	0.2	14.4	7.9	6.3	0.4	-0.2	0.2
Mar	4.4	2.2	2.2	0.3	-0.3	0.1	14.1	7.8	6.3	0.4	-0.3	0.0
Apr	4.3	2.2	2.2	0.5	-0.6	-0.1	13.9	7.9	6.3	0.5	-0.8	-0.3
May	3.9	2.2	2.2	0.7	-1.2	-0.5	13.9	7.9	6.3	0.8	-1.0	-0.3
Jun	1.2	2.2	2.2	0.9	-4.0	-3.2	10.9	7.8	6.2	1.0	-4.1	-3.2
Jul	0.0	2.2	2.2	1.1	-5.6	-4.5	9.1	7.9	6.3	1.2	-6.3	-5.1
Aug	1.7	2.2	2.2	0.9	-3.6	-2.6	11.2	7.8	6.3	1.0	-4.0	-3.0
Sep	3.1	2.2	2.2	0.6	-2.0	-1.4	12.6	7.8	6.3	0.7	-2.3	-1.5
Oct	4.7	2.2	2.2	0.6	-0.3	0.2	14.5	7.9	6.3	0.7	-0.4	0.3
Nov	4.7	2.1	2.1	0.4	-0.1	0.3	14.5	7.8	6.3	0.5	-0.1	0.4
Dec	4.8	2.2	2.2	0.3	0.0	0.3	14.5	7.8	6.3	0.4	0.0	0.4
Year	3.5	2.2	2.2	0.6	-1.5	-0.9	13.2	7.9	6.3	0.7	-1.6	-1.0

4.4 Diurnal variation

Figure 4.10 and Figure 4.11 display the diurnal behaviour of simulated CO_2 fluxes and the components contributing to the net CO_2 emissions in different seasons under previous and future scenarios, respectively. The pattern of diurnal variation of traffic and metabolism remains similar in all seasons with high values in the daytime and low values in the nocturnal. Road traffic and human metabolism are the two dominant sources of CO_2 emissions. The CO_2 emissions due to soil and vegetation respiration are maintained stable for the whole day and much lower than the other two sources. The photosynthesis sink of CO_2 is strong in the daytime when the incoming shortwave radiation is high. Obviously, the range of diurnal variation of CO_2 sink increases in summer.

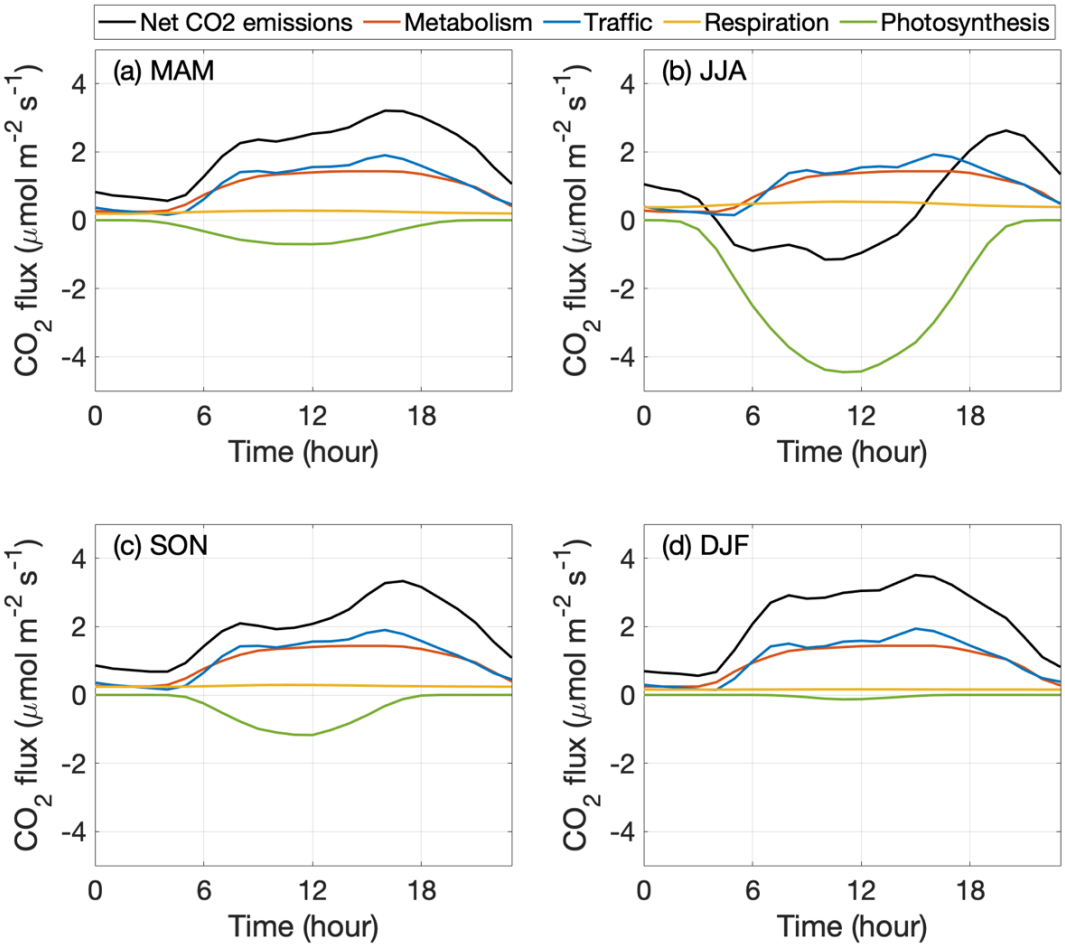

Figure 4.11 Mean diurnal variation of modeled CO_2 flux and its components (metabolism, traffic, respiration, and photosynthesis) in Jätkäsaari for different seasons: (a) spring, (b) summer, (c) autumn, and (d) winter in 2008.

In the 2008 case, the CO_2 emission from traffic decreases during the nighttime and reduces to around 0.15 μmol m^{-2} s-1 in the early morning. Then, it increases as the rising traffic volumes and reaches a maximum value of 1.9 μmol m^{-2} s^{-1}in the afternoon. It presents a slight bimodal distribution because of rush hours. The maximum of photosynthesis CO_2 sink reaches -4.5 μmol m^{-2} s^{-1} at 11:00 on a summer day. The diurnal behaviour of net CO_2 flux stays a similar pattern with peaks in 4:00-5:00 in the afternoon. The exception occurs in the summer period when photosynthesis sink exceeds the emissions from the early morning to the afternoon, resulting negative net CO_2 fluxes from 5:00 to 14:00.

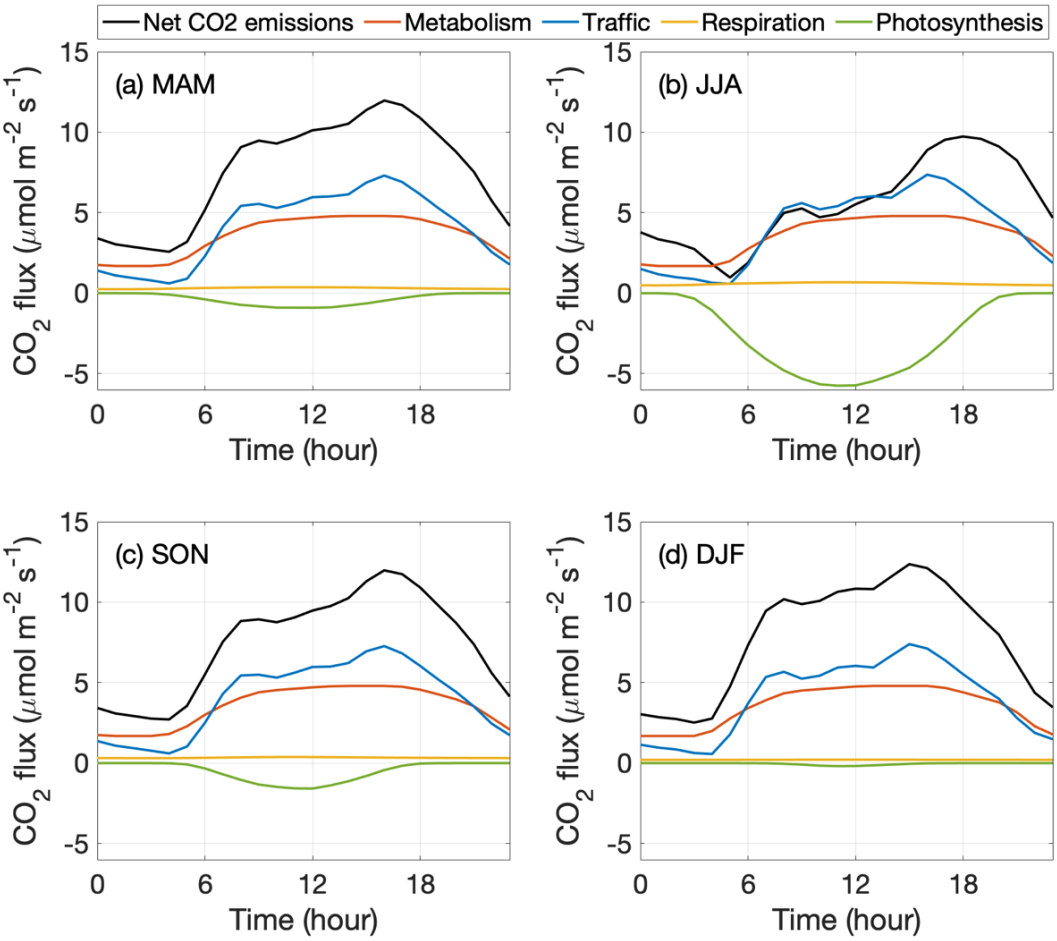

Figure 4.12 Mean diurnal variation of modeled CO_2 flux and its components (metabolism, traffic, respiration, and photosynthesis) in Jätkäsaari for different seasons: (a) spring, (b) summer, (c) autumn, and (d) winter in 2030.

In the future case, the bimodal patterns are also obvious for diurnal variation of the traffic CO_2 emissions in all season. The traffic CO_2 emission is maintained a low value less than 1.5

μmol m^{-2} s^{-1} during nighttime and begins to increase in the early morning. It reaches the maximum value of around 7.3 μmol m^{-2} s^{-1} in the afternoon rush hour. The net CO_2 flux reduces during the nighttime, and in the early morning, it shifts to increase. In all seasons, the averaged net CO_2 flux is positive even if the photosynthesis sink intensifies in the summertime.

4.5 Contrast of CO_2 emissions between 2008 and 2030

Impacts of the urban planning involving the surface cover change, increased inhabitants, and rising traffic on CO_2 emission are summarized in detail in this section.

In the study area, total CO_2 emissions increase from 3.5 kt CO_2 year-1 to 13.2 kt CO_2 year $^{-1}$. Since the net biogenic CO_2 flux remains -0.9 kt C $year^{-1}$, the anthropogenic emissions contribute to almost all the enhancement. The increment of traffic volume from Jätkäsaari to city centre is predicted to be 18000 veh day^{-1} according to Helsinki City Planning Department. Owing to this dramatic increase, transportation becomes the most important CO_2 sources and takes up 53% of the total emissions in 2030, while this value is 44% in 2008.

Based on the distribution of annual accumulative net CO_2 emissions (Figure 4.8), positive values appear in more grids in the model domain in the future, which implies that more grids become the CO_2 source. The dense residential blocks and increasing inhabitants in the urban planning results in the CO_2 emission from human metabolism dominates majority of the grid emission. Although the fraction of vegetation in model domain increase slightly in 2030, the number of grids which can acts as CO_2 sinks reduce a lot. CO_2 sink areas are only located at the greenspace in park and along the southwest coast, where there is no traffic road, as well as no residential and commercial building.

The impacts of urban planning on CO_2 emissions reflect more in the spatial variability than in the temporal variability. The behaviour of the monthly and seasonal variation of CO_2 emissions in 2030 is similar to that in 2008. The differences are mainly concentrated on the increase of the anthropogenic CO_2 emissions. For example, in summertime, the CO_2 emission from human metabolism increases from 2.2 g CO_2 m^{-2} day^{-1} to 6.3 g CO_2 m^{-2} day^{-1}, and the CO_2 emission from traffic enhances from 2.2 g CO_2 m^{-2} day^{-1} to 7.9 g CO_2 m^{-2} day^{-1}. However, the differences in CO_2 fluxes from biogenic components are not significant between 2008 and 2030.

5 Conclusion

This study aims at estimating the CO_2 emissions from different source sectors including traffic, human metabolism, soil and vegetation respiration, and photosynthesis in past and future Jätkäsaari, Helsinki, and further examininng the impacts of urban planning on local CO_2 emissions. The study area, Jätkäsaari, started to be constructed from 2009 and planned to be completed in 2030 according to Helsinki city plan. The urban land surface model SUEWS incorporated with a CO2 exchange module is conducted in a 1650 × 1400 m domain with the spatial resolution of 50 × 50 m and the time resolution of an hour to study the total areal CO_2 emissions, and the temporal and spatial variation of CO_2 fluxes in 2008 and 2030. The focus is laid on implementing the model in a real case, and preprocessing various urban surface information involving urban planning map, traffic data, nighttime and daytime population density into model input.

The total amount of CO_2 released into the atmosphere from the study area is 3.0 kt per year in 2008, of which 1.9 kt is from traffic, 1.9 kt is from metabolism, 0.5 kt is from soil and vegetation respiration, -1.3 kt is due to photosynthesis. In 2030, the total CO_2 flux in study region increased to 11.1 kt CO_2 $year^{-1}$. The largest exchange contributor is traffic of 6.6 kt CO_2 $year^{-1}$, followed by metabolism of 5.3 kt CO_2 $year^{-1}$, photosynthesis of -1.4 kt CO_2 $year^{-1}$, and respiration of 0.6 kt CO_2 $year^{-1}$. The increase of areal CO_2 emissions results from the rising anthropogenic emissions as the biogenic net CO_2 fluxes remain the same.

The spatial variability of net CO_2 fluxes is dominated by the distribution of CO_2 fluxes from traffic and metabolism. The hotspots of CO_2 emissions appear in areas including high traffic volumes, as well as dense residential and commercial buildings with people. In the whole region, the net biogenic CO_2 flux is negative, which indicates that the biogenic components act as a CO_2 sink in Jätkäsaari. In 2008, as most of the study area is the waste land, CO_2 flux from vegetation dominates the total emission in a majority of the grids. However, in 2030, as the population density increased over the study areas, CO_2 flux form human metabolism dominates the CO_2 emissions in most grids except for main road and park areas.

On a monthly basis, the anthropogenic CO_2 emissions are stable with values of 4.4 g CO_2 m^{-2} day^{-1} and 14.2 g CO_2 m^{-2} day^{-1} in 2008 and 2030, respectively. The vegetation acts as the CO_2 sink with negative net ecosystem exchange from April to September both in 2008 and 2030. On a daily basis, in spring, autumn and winter, the diurnal behaviour of the net CO_2 flux presents a bimodal mode because of rush hours. In 2008, the study area remains the CO_2

sources with the exception of summertime morning when the net CO_2 flux is negative, while in 2030, the net CO_2 flux is positive in the whole day. In summary, the impacts of urban planning on CO_2 emissions reflect more in the spatial variability of CO_2 fluxes than in the temporal variability.

References

Ahmadov, R., Gerbig, C., Kretschmer, R., Körner, S., Rödenbeck, C., Bousquet, P., & Ramonet, M. (2009). Comparing high resolution WRF-VPRM simulations and two global CO 2 transport models with coastal tower measurements of CO_2. *Biogeosciences*, 6, 807-817.

Arnfield, A. J. (2003). Two decades of urban climate research: A review of turbulence, exchanges of energy and water, and the urban heat island. *International Journal of Climatology*, 23, 1-26.

Baldocchi, D. D. (2003). Assessing the eddy covariance technique for evaluating carbon dioxide exchange rates of ecosystems: Past, present and future. *Global Change Biology*, 9, 479-492.

Barlow, J. F. (2014). Progress in observing and modelling the urban boundary layer. *Urban Climate*.

Bellucco, V., Marras, S., Grimmond, C. S. B., Järvi, L., Sirca, C., & Spano, D. (2017). Modelling the biogenic CO_2 exchange in urban and non-urban ecosystems through the assessment of light-response curve parameters. *Agricultural and Forest Meteorology*, 236, 113-122.

Bergamaschi, P., Danila, A., Weiss, R. F., Ciais, P., Thompson, R. L., Brunner, D., … Vogel, F. (2018). Atmospheric monitoring and inverse modelling for verification of greenhouse gas inventories. In *European Commission*.

Bergeron, O., & Strachan, I. B. (2011). CO_2 sources and sinks in urban and suburban areas of a northern mid-latitude city. *Atmospheric Environment*, 45, 1564-1573.

Björkegren, A., & Grimmond, C. S. B. (2018). Net carbon dioxide emissions from central London. *Urban Climate*, 23, 131-158.

Blunden, J., & Arndt, D., Eds. (2019). State of the climate in 2018. *Bulletin of the American Meteorological Society*.

Brondfield, M. N., Hutyra, L. R., Gately, C. K., Raciti, S. M., & Peterson, S. A. (2012). Modeling and validation of on-road CO 2 emissions inventories at the urban regional scale. *Environmental Pollution*, 170, 113-123.

Christen, A., Coops, N. C., Crawford, B. R., Kellett, R., Liss, K. N., Olchovski, I., … Voogt, J. A. (2011). Validation of modeled carbon-dioxide emissions from an urban neighborhood with direct eddy-covariance measurements. *Atmospheric Environment*, 45, 6057-6069.

Feng, S., Lauvaux, T., Newman, S., Rao, P., Ahmadov, R., Deng, A., … Yung, Y. L. (2016). Los Angeles megacity: A high-resolution land-atmosphere modelling system for urban CO_2 emissions. *Atmospheric Chemistry and Physics*, 16, 9019-9045.

Finnish Transport and Communications Agency. More than three million passenger cars registered in Finland – steady increase in vehicles with alternative driving power. Access date: 21.05.2020. Retrieved from: https://arkisto.trafi.fi/en/news/5350/more_than_three_million_passenger_cars_registered_in_finland_-_steady_increase_in_vehicles_with_alternative_driving_power.

Gately, C. K., & Hutyra, L. R. (2017). Large Uncertainties in Urban-Scale Carbon Emissions. *Journal of Geophysical Research: Atmospheres*, 122, 11242-11260.

Grimmond, C. S. B., & Oke, T. R. (1991). An evapotranspiration-interception model for urban areas. *Water Resources Research*, 27, 1739-1755.

Grimmond, C. S. B., & Oke, T. R. (2002). Turbulent heat fluxes in urban areas: Observations and a local-scale urban meteorological parameterization scheme (LUMPS). *Journal of Applied Meteorology*, 41, 792-810.

Hardiman, B. S., Wang, J. A., Hutyra, L. R., Gately, C. K., Getson, J. M., & Friedl, M. A. (2017). Accounting for urban biogenic fluxes in regional carbon budgets. *Science of the Total Environment*, 592, 366-372.

Helsinki City Planning Department. (2008) Jätkäsaari, osayleiskaava selostus.

Holton, J. R., & Hakim, G. J. (2012). An introduction to dynamic meteorology: Fifth edition.

HEL. (2017). City Surveying Department, autumn weekday traffic in Helsinki 2016. Access date: 21.05.2020. Retrieved from: https://www.hel.fi/hel2/ksv/Aineistot/ Liikennesuunnittelu/Liikennetutkimus/Liikennemaarat.pdf.

HSY. (2011). SeutuCD'11 database. Helsinki Region Environmental Services Authority.

IPCC. (2014). Climate Change 2014: Synthesis Report. Contribution of Working Groups I, II and III to the Fifth Assessment Report of the Intergovernmental Panel on Climate Change [Core Writing Team, R.K. Pachauri and L.A. Meyer (eds.)]. IPCC, Geneva, Switzerland.

International Energy Agency. (2008) World Energy Outlook 2008, International Energy Agency, Paris.

Järvi, L., Grimmond, C. S. B., & Christen, A. (2011). The Surface Urban Energy and Water Balance Scheme (SUEWS): Evaluation in Los Angeles and Vancouver. *Journal of Hydrology*, 411, 219-237.

Järvi, L., Nordbo, A., Junninen, H., Riikonen, A., Moilanen, J., Nikinmaa, E., & Vesala, T. (2012). Seasonal and annual variation of carbon dioxide surface fluxes in Helsinki, Finland, in 2006-2010. *Atmospheric Chemistry and Physics*, 12, 8475-8489.

Järvi, L., Grimmond, C. S. B., Taka, M., Nordbo, A., Setälä, H., & Strachan, I. B. (2014). Development of the Surface Urban Energy and Water Balance Scheme (SUEWS) for cold climate cities. *Geoscientific Model Development*, 7, 1691-1711.

Järvi, L., Havu, M., Ward, H. C., Bellucco, V., McFadden, J. P., Toivonen, T., … Grimmond, C. S. B. (2019). Spatial Modeling of Local-Scale Biogenic and Anthropogenic Carbon Dioxide Emissions in Helsinki. *Journal of Geophysical Research: Atmospheres*, 124, 8363-8384.

Kennedy, C., Steinberger, J., Gasson, B., Hansen, Y., Hillman, T., Havránek, M., … Mendez, G. V. (2009). Greenhouse gas emissions from global cities. *Environmental Science and Technology*, 3, 7297-7302.

Kurppa, M., Nordbo, A., Haapanala, S., & Järvi, L. (2015). Effect of seasonal variability and land use on particle number and CO_2 exchange in Helsinki, Finland. *Urban Climate*, 13, 94-109.

Lasslop, G., Reichstein, M., Papale, D., Richardson, A., Arneth, A., Barr, A., … Wohlfahrt, G. (2010). Separation of net ecosystem exchange into assimilation and respiration using a light response curve approach: Critical issues and global evaluation. *Global Change Biology*, 187-208.

Lauvaux, T., Miles, N. L., Deng, A., Richardson, S. J., Cambaliza, M. O., Davis, K. J., … Wu, K. (2016). High-resolution atmospheric inversion of urban CO_2 emissions during the dormant season of the Indianapolis flux experiment (INFLUX). *Journal of Geophysical Research*, 121, 5213-5236.

Lin, J. C., Mitchell, L., Crosman, E., Mendoza, D. L., Buchert, M., Bares, R., … Ehleringer, J. (2018). CO_2 and carbon emissions from cities linkages to air quality, socioeconomic activity, and stakeholders in the Salt Lake City urban area. *Bulletin of the American Meteorological Society*.

Makido, Y., Dhakal, S., & Yamagata, Y. (2012). Relationship between urban form and CO_2 emissions: Evidence from fifty Japanese cities. *Urban Climate*, 2, 55-67.

Mäkelä, A., Kolari, P., Karimäki, J., Nikinmaa, E., Perämäki, M., & Hari, P. (2006). Modelling five years of weather-driven variation of GPP in a boreal forest. *Agricultural and Forest Meteorology*, 139, 382-398.

Mäkelä, A., Pulkkinen, M., Kolari, P., Lagergren, F., Berbigier, P., Lindroth, A., … Hari, P. (2008). Developing an empirical model of stand GPP with the LUE approach: Analysis of eddy covariance data at five contrasting conifer sites in Europe. *Global Change Biology*, 14,92-108.

Menzer, O., & McFadden, J. P. (2017). Statistical partitioning of a three-year time series of direct urban net CO_2 flux measurements into biogenic and anthropogenic components. *Atmospheric Environment*, 170,319-333.

Moriwaki, R., & Kanda, M. (2004). Seasonal and diurnal fluxes of radiation, heat water vapor, and carbon dioxide over a suburban area. *Journal of Applied Meteorology*, 43,1700-1710.

Nejadkoorki, F., Nicholson, K., Lake, I., & Davies, T. (2008). An approach for modelling CO_2 emissions from road traffic in urban areas. *Science of the Total Environment*, 406, 269-278.

Nordbo, A., Järvi, L., Haapanala, S., Wood, C. R., & Vesala, T. (2012). Fraction of natural area as main predictor of net CO_2 emissions from cities. *Geophysical Research Letters*, 39, L20802.

Nordbo, A., Järvi, L., & Vesala, T. (2012). Revised eddy covariance flux calculation methodologies-effect on urban energy balance. Tellus, Series B: *Chemical and Physical Meteorology*, 64, 18184.

Nordbo, A., Karsisto, P., Matikainen, L., Wood, C. R., & Järvi, L. (2015). Urban surface cover determined with airborne lidar at 2m resolution - Implications for surface energy balance modelling. *Urban Climate*, 13, 52-72.

Offerle, B., Grimmond, C. S. B., & Oke, T. R. (2003). Parameterization of net all-wave radiation for urban areas. *Journal of Applied Meteorology*, 42,1157-1173.

Oke, T. R. (1987). Boundary layer climates, Second edition. Routledge, London, UK.

Oke, T. R., Mills, G., Christen, A., & Voogt, J. A. (2017). Urban climates.

Ögren, E., & Evans, J. R. (1993). Photosynthetic light-response curves - I. The influence of CO_2 partial pressure and leaf inversion. *Planta*, 189, 182-190.

Pacheco-Torres, R., Roldán, J., Gago, E. J., & Ordóñez, J. (2017). Assessing the relationship between urban planning options and carbon emissions at the use stage of new urbanized areas: A case study in a warm climate location. *Energy and Buildings*, 136, 73-85.

Pino, D., & Vilà-Guerau de Arellano, J. (2010). Role of boundary layer processes on the mixed layer CO_2-budget. *19th Symposium on Boundary Layers and Turbulence and the 29th Conference on Agricultural and Forest Meteorology*; Keystone, Colorado, USA

Reckien, D., Ewald, M., Edenhofer, O., & Lüdeke, M. K. B. (2007). What parameters influence the spatial variations in CO_2 emissions from road traffic in Berlin? Implications for urban planning to reduce anthropogenic CO_2 emissions. *Urban Studies*, 44, 339-355.

Ribeiro, H. V., Rybski, D., & Kropp, J. P. (2019). Effects of changing population or density on urban carbon dioxide emissions. *Nature Communications*.

Ryu, Y. H., & Baik, J. J. (2012). Quantitative analysis of factors contributing to urban heat island intensity. *Journal of Applied Meteorology and Climatology*, 51, 842-854.

Sailor, D. J., & Lu, L. (2004). A top-down methodology for developing diurnal and seasonal anthropogenic heating profiles for urban areas. *Atmospheric Environment*, 38, 2737-2748.

Sargent, M., Barrera, Y., Nehrkorn, T., Hutyra, L. R., Gately, C. K., Jones, T., … Wofsy, S. C. (2018). Anthropogenic and biogenic CO_2 fluxes in the Boston urban region. *Proceedings of the National Academy of Sciences of the United States of America,* 29, 7491-7496.

Satterthwaite, D. (2008). Cities' contribution to global warming: Notes on the allocation of greenhouse gas emissions. *Environment and Urbanization*, 20, 539-549.

Song, T., Wang, Y., & Sun, Y. (2013). Estimation of carbon dioxide flux and source partitioning over Beijing, China. *Journal of Environmental Sciences*, 25, 2429-2434.

Stull, R. B. (1988). An introduction to boundary layer meteorology. An Introduction to Boundary Layer Meteorology.

Sun, Ting, Järvi, Leena, Grimmond, C.S.B., Lindberg, Fredrik, Li, Zhenkun, Tang, Yihao, & Ward, Helen. (2019, February 21). SUEWS Documentation (Version 2018c). Zenodo.

Uutta Helsinkiä, Jätkäsaari. Retrieved from: https://www.uuttahelsinkia.fi/fi/jatkasaari. Access date: 21.05.2020.

Velasco, E., Perrusquia, R., Jiménez, E., Hernández, F., Camacho, P., Rodríguez, S., … Molina, L. T. (2014). Sources and sinks of carbon dioxide in a neighborhood of Mexico City. *Atmospheric Environment*, 97, 226-238.

Wang, L., Li, D., Gao, Z., Sun, T., Guo, X., & Bou-Zeid, E. (2014). Turbulent Transport of Momentum and Scalars Above an Urban Canopy. *Boundary-Layer Meteorology*, 150, 485-511.

Wang, S. H., Huang, S. L., & Huang, P. J. (2018). Can spatial planning really mitigate carbon dioxide emissions in urban areas? A case study in Taipei, Taiwan. *Landscape and Urban Planning*, 169, 22-36, 169, 22-36.

Ward, H. C., Evans, J. G., & Grimmond, C. S. B. (2013). Multi-season eddy covariance observations of energy, water and carbon fluxes over a suburban area in Swindon, UK. *Atmospheric Chemistry and Physics*, 13, 4645–4666.

Ward, H. C., Kotthaus, S., Grimmond, C. S. B., Bjorkegren, A., Wilkinson, M., Morrison, W. T. J., … Iamarino, M. (2015). Effects of urban density on carbon dioxide exchanges: Observations of dense urban, suburban and woodland areas of southern England. *Environmental Pollution*, 198, 186-200.

Ward, H. C., Kotthaus, S., Järvi, L., & Grimmond, C. S. B. (2016). Surface Urban Energy and Water Balance Scheme (SUEWS): Development and evaluation at two UK sites. *Urban Climate*, 18, 1-32.

Zhang, K., Gong, Y., Fa, H., & Zhao, M. (2019). CO_2 flux characteristics of different plant communities in a subtropical urban ecosystem. *Sustainability*, 11,4879.